



Aberrant Whole-Brain Transitions and Dynamics of Spontaneous Network Microstates in Mild Traumatic Brain Injury

Marios Antonakakis^{1,2,3*}, Stavros I. Dimitriadis^{4,5,6,7,8}, Michalis Zervakis², Andrew C. Papanicolaou⁹ and George Zouridakis¹⁰

¹ Institute for Biomagnetism and Biosignal Analysis, University of Muenster, Muenster, Germany, ² Digital Image and Signal Processing Laboratory, School of Electronic and Computer Engineering, Technical University of Crete, Chania, Greece, ³ Neuroinformatics Group, Cardiff University Brain Research Imaging Center (CUBRIC), School of Psychology, Cardiff University, Cardiff, United Kingdom, ⁴ Institute of Psychological Medicine and Clinical Neurosciences, Cardiff University School of Medicine, Cardiff, United Kingdom, ⁵ Cardiff University Brain Research Imaging Center (CUBRIC), School of Psychology, Cardiff University, Cardiff, United Kingdom, ⁶ School of Psychology, Cardiff University, Cardiff, United Kingdom, ⁷ Neuroscience and Mental Health Research Institute, Cardiff University, Cardiff, United Kingdom, ⁸ MRC Centre for Neuropsychiatric Genetics and Genomics, School of Medicine, Cardiff University, Cardiff, United Kingdom, ⁹ Departments of Pediatrics, and Anatomy and Neurobiology, Neuroscience Institute, University of Tennessee Health Science Center, Le Bonheur Children's Hospital, Memphis, TN, United States, ¹⁰ Biomedical Imaging Lab, Departments of Engineering Technology, Computer Science, Biomedical Engineering, and Electrical and Computer Engineering, University of Houston, Houston, TX, United States

OPEN ACCESS

Edited by:

Maurizio Mattia,
Istituto Superiore di Sanità (ISS), Italy

Reviewed by:

Alessio Basti,
Università degli Studi G. d'Annunzio
Chieti e Pescara, Italy
Duan Li,
University of Michigan, United States

*Correspondence:

Marios Antonakakis
marios.antonakakis@uni-muenster.de;
antonakakismar@gmail.com

Received: 22 September 2019

Accepted: 19 December 2019

Published: 15 January 2020

Citation:

Antonakakis M, Dimitriadis SI, Zervakis M, Papanicolaou AC and Zouridakis G (2020) Aberrant Whole-Brain Transitions and Dynamics of Spontaneous Network Microstates in Mild Traumatic Brain Injury. *Front. Comput. Neurosci.* 13:90. doi: 10.3389/fncom.2019.00090

Dynamic Functional Connectivity (DFC) analysis is a promising approach for the characterization of brain electrophysiological activity. In this study, we investigated abnormal alterations due to mild Traumatic Brain Injury (mTBI) using DFC of the source reconstructed magnetoencephalographic (MEG) resting-state recordings. Brain activity in several well-known frequency bands was first reconstructed using beamforming of the MEG data to determine ninety anatomical brain regions of interest. A DFC graph was formulated using the imaginary part of phase-locking values, which were obtained from 30 mTBI patients and 50 healthy controls (HC). Subsequently, we estimated normalized Laplacian transformations of individual, statistically and topologically filtered quasi-static graphs. The corresponding eigenvalues of each node synchronization were then computed and through the neural-gas algorithm, we quantized the evolution of the eigenvalues resulting in distinct network microstates (NMstates). The discrimination level between the two groups was assessed using an iterative cross-validation classification scheme with features either the NMstates in each frequency band, or the combination of the so-called chronnectomics (flexibility index, occupancy time of NMstate, and Dwell time) with the complexity index over the evolution of the NMstates across all frequency bands. Classification performance based on chronnectomics showed 80% accuracy, 99% sensitivity, and 49% specificity. However, performance was much higher (accuracy: 91–97%, sensitivity: 100%, and specificity: 77–93%) when focusing on the microstates. Exploring the mean node degree within and between brain anatomical networks (default mode network, frontoparietal, occipital, cingulo-opercular, and sensorimotor), a reduced pattern occurred from lower to higher frequency bands, with statistically significant stronger degrees for the HC than the mTBI group. A higher entropic profile on the

temporal evolution of the modularity index was observed for both NMstates for the mTBI group across frequencies. A significant difference in the flexibility index was observed between the two groups for the β frequency band. The latter finding may support a central role of the thalamus impairment in mTBI. The current study considers a complete set of frequency-dependent connectomic markers of mTBI-caused alterations in brain connectivity that potentially could serve as markers to assess the return of an injured subject back to normality.

Keywords: MEG, mTBI, beamforming, dynamic functional connectivity analysis, network microstates, symbolic dynamics, chronnectomics, connectomic biomarkers

INTRODUCTION

Mild traumatic brain injury (mTBI) accounts for ~90% of all brain injuries (Len and Neary, 2011), establishing it as a major cause of brain insult (Huang et al., 2014). A considerable part of mTBI patients develops persistent cognitive deficits (van der Naalt et al., 1999; Vanderploeg et al., 2005), and post-concussion symptoms can cause irremediable problems in ~20% of the patients (Bharath et al., 2016) several months after the first injury (Huang et al., 2014). The main characteristics of those symptoms are often physical, emotional, cognitive, and sleep disturbances that may need several months to improve (Huang et al., 2014). In many neuropsychological studies (Huang et al., 2014; Pang et al., 2016), reduced cognitive efficiency in several brain functions has been reported, especially in tests measuring processing speed, executive function, attention, memory, and connectivity, in mTBI patients with persistent symptoms. Handling of mTBI patients is not a trivial task as oftentimes mTBI affects severely brain functionality (Vanderploeg et al., 2005; De Monte et al., 2006). In the present study, we aim to reveal abnormal alterations due to mTBI using magnetoencephalographic resting-state data and dynamic functional connectivity (DFC) patterns in source space.

Conventional structural neuroimaging, such as computed tomography (CT) and acute magnetic resonance imaging (MRI), as well as functional MRI (fMRI) usually offer low sensitivity for detecting physiological alterations caused by mTBI (Kirkwood et al., 2006). A recent study (Vergara et al., 2018) revealed high classification levels of mTBI subjects exploiting time resolved connectivity profiles but with temporal limitations due to the use of fMRI. Magnetoencephalography (MEG) is a non-invasive functional imaging modality that detects activity from the synchronous oscillations of neurons' membranes in the gray matter. Thus, MEG incorporates high sensitivity by keeping the environmental noise to a low level, and includes low-resolution spatial details and high temporal accuracy (Leahy et al., 1998). In this study, we combined for the first time the reconstructed source MEG activity with the notion of functional connectivity (FC) for the characterization of mTBI over time. FC is crucial for the characterization of most brain disorders (Eierud et al., 2014; Baillet, 2017). The term FC was introduced when the human brain was first modeled as a neurophysiological network with functional communication among several anatomical areas. These distinct networks can exist in a range of spatiotemporal scales with spatial diversity and

temporal variability. Spatially, these networks can vary between microscopic neuronal aggregates and large-scale interconnected brain areas (Eierud et al., 2014).

Several studies, including ours, have recently investigated the development of robust biomarkers for detecting mTBI using MEG or fMRI and under the notion of FC (Huang et al., 2009; Castellanos et al., 2010; see reviews by Jeter et al., 2013; and Eierud et al., 2014; Da Costa et al., 2015; Dunkley et al., 2015; Vakorin et al., 2016). More recently, Dunkley et al. (2018) investigated the impact of the injury on intrinsic connectivity networks and showed increased coupling in the default mode network of mTBI patients. Dimitriadis et al. (2015), using phase-coupling, quantified intra-frequency couplings at the sensor level and found significantly different patterns that were seen mostly in the delta band, whereas Alhourani et al. (2016) used the same metric at the source level and showed reduced local efficiency in different brain regions in mTBI patients. In a series of follow-up studies, we (Antonakakis et al., 2016, 2017a) showed less dense connectivity networks in mTBI patients, which was in line with the findings of other groups (Rapp et al., 2015), as well as higher synchronization among mTBI rich-club hubs (Antonakakis et al., 2017b). More recently, Li et al. (2018) revealed a denser causality network for mTBI patients, whereas Kaltiainen et al. (2018) showed that aberrant theta-band activity could provide an early objective sign of brain abnormality after mTBI.

MEG-based FC is an emerging procedure in the development of reliable mTBI biomarkers using resting-state networks (RSNs), not only at the sensor level, but also at the source level, since source level RSNs have been successfully estimated in the past few years (Brookes et al., 2011a,b; Hipp et al., 2012; Luckhoo et al., 2012; Hall et al., 2013; Wens et al., 2015). MEG-based RSNs form a promising approach for detecting several other brain functional abnormalities, involving dyslexia (Dimitriadis et al., 2016), mild cognitive impairment (Maestú et al., 2015), and multiple sclerosis (Tewarie et al., 2015). However, the use of RSNs as short-lived transient brain states (van Dijk et al., 2010) varies significantly across different studies, ranging from estimating the MEG frequency spectrum (Vidaurre et al., 2016) to band-specific amplitude envelopes of reconstructed MEG sources (Baker et al., 2014; O'Neill et al., 2015; Vidaurre et al., 2016). A recent neuroimaging index, called chronnectomics (Allen et al., 2012; Calhoun and Adali, 2016), was proposed in fMRI studies to express the synergy between time-varying FC and the

evolution of distinct spatiotemporal alternations among various brain states.

In this study, we investigated whole-brain dynamic FC (DFC) derived from MEG resting-state data from 80 subjects (50 HC and 30 mTBI). To our knowledge, this is the first study that utilizes DFC on reconstructed MEG source activity for the investigation of mTBI. Similar methodological aspects have been adopted in other recent studies with normal controls and mild cognitive impairment subjects (Dimitriadis et al., 2018a).

Within brain interactions were modeled using beamformed MEG source activation and DFC among ninety atlas-based brain areas using a template MRI. Each quasi-static FC was determined by the imaginary part of the phase locking value (iPLV) (Dimitriadis et al., 2018a; Palva et al., 2018), and it was filtered statistically and topologically (Dimitriadis et al., 2017) to reduce spurious connections. Subsequently, we coded the estimated time-varying network activity into prototypical network microstates or NMstates (Dimitriadis et al., 2013, 2018a). Through this approach, we derived symbolic-form time series for which the chronnectomic behavior was modeled based on the metric transition rate of NMstates, fractional occupancy of each NMstate, Dwell time, and complexity index (Dimitriadis et al., 2018b). Finally, we assessed DFC differentiations of mTBI subjects using statistical inference and classification.

The rest of the paper is organized as follows: section Materials and Methods describes in detail the study participants, data acquisition, preprocessing steps, the methodological approach, and the resulting chronnectomics. Section Results is devoted to the description of findings based on the frequency-dependent prototypical network NMstates and the extracted chronnectomics. Section Discussion includes a discussion on the analysis results in the context of the current literature, and its potential impact on the field. Finally, section Discussion summarizes the conclusions of the study and presents possible future extensions.

MATERIALS AND METHODS

Participants and Recordings

The current study included data from 50 right-handed healthy controls (HC) (29.25 ± 9.1 years of age) and 30 right-handed mTBI patients (29.33 ± 9.2 years of age). The participants gave written informed consent to the study. All clinical information, including the selection criteria, was reviewed and provided by board certified clinicians. **Table 1** summarizes patient demographics. Controls were recruited from a normative data repository at UTHSC-Houston and were particularly selected so that they were age-matched with the mTBI group. The selected healthy control subjects had no previous head injuries, extensive dental work, substance abuse, history of neurologic or psychiatric disorder, or implants incompatible with MEG. Prior to the present study, the research protocol received institutional approval. The mTBI patients were recruited from three trauma centers in the greater Houston metropolitan area that participated in a larger study (Zouridakis et al., 2012). Further details can be found elsewhere (Zouridakis et al., 2012; Dimitriadis et al., 2015; Antonakakis et al.,

2016). Characterization of mTBI patients was based on the guidelines of the American Congress of Rehabilitation Medicine (Kay et al., 1993) and the Department of Defense (Assistant Secretary, 2007). Institutional Review Board (IRB) approval for the project was obtained at the participating institutions and the Human Research Protection Official's review of research protocols for the Department of Defense. All procedures were fully compliant with the Health Insurance Portability and Accountability Act (HIPAA).

Spontaneous MEG activity was acquired with a whole-head Magnes WH3600 system of 248 axial gradiometers (4D Neuroimaging Inc., San Diego, CA) for 10 min at a sampling rate of 1,017.25 Hz. An online bandpass filter between 0.1 and 200 Hz was applied to reduce noise effects. No independent ocular or cardiac activity was recorded. Subjects were in a supine position with eyes closed during data acquisition. After excluding activity contaminated with artifacts (Dimitriadis et al., 2015) and conversion from axial gradiometer recordings to planar gradiometer field approximations in FieldTrip (Oostenveld et al., 2011), ~ 5 min of clean data were used for further analysis.

MEG Pre-processing

Artifact reduction in the MEG recordings was accomplished with an automated detection and elimination procedure described in detail elsewhere (Antonakakis et al., 2017a) that was based on the FieldTrip software (Oostenveld et al., 2011) implemented in MATLAB (The MathWorks, Inc., Natick, MA, USA). In brief, noisy activity was attenuated using the following steps: (1) correction of bad MEG channel activity by applying interpolation techniques, (2) elimination of frequencies outside the range 0.1–100 Hz using digital filtering, (3) elimination of the power line noise at 60 Hz with a notch filter, and (4) detection and elimination of electrophysiological (ocular and cardiac) artifacts by first decomposing the MEG signals into statistically independent components (Delorme and Makeig, 2004) and then applying combined fixed thresholds on the statistical values of kurtosis, skewness, and Rényi entropy as described in detail elsewhere (Antonakakis et al., 2017a).

Source Analysis

Atlas-based beamforming was used for reconstructing source activity from MEG measurements. The investigated frequency bands included δ (0.5–4 Hz), θ (4–8 Hz), α_{low} (8–10 Hz), α_{high} (10–13 Hz), β (13–30 Hz), γ_{low} (30–55 Hz), and γ_{high} (55–90 Hz). First, the MEG sensor locations of each subject were realigned with a standard T1-weighted MRI template of 2 mm resolution provided by SPM8 (Weiskopf et al., 2011). The division of the MRI anatomical areas into 90 brain regions of interest (ROIs) was performed based on the Automated Anatomical Labeling (AAL) atlas (Hillebrand and Barnes, 2002; Tzourio-Mazoyer et al., 2002; Hillebrand et al., 2016; Hunt et al., 2016). We employed a spherical head model (Nolte et al., 2004) that included 5,061 sources (6 mm resolution) and covered the entire brain tissue. Frequency-dependent MEG source activity was reconstructed using the linearly constrained minimum norm variance (LCMV) algorithm in FieldTrip (Oostenveld et al., 2011).

TABLE 1 | Patient demographics for the mTBI group.

Age at injury (min—max)	Males (females)	Auto pedestrian—frontal (# subjects)	Auto pedestrian—frontal—type (# subjects)	Auto pedestrian—frontal—location (# subjects)
(19–25)	7 (5)	Assault (2), Motor Vehicle (5), Sports-related (2), Auto Pedestrian (1), ATV (1), Assault (1)	Contusion (4), Bruising (3), Laceration—no sutures (1), Tenderness (2), Laceration—with sutures (2)	Head (10), Head/Face (2)
(25–40)	8 (2)	Fall (1), Auto Pedestrian (2), Fall Moving Object (1), Assault (1), Motor Vehicle (1), Fall Raised Surface (2), Assault (1), Blow to Head (1)	Abrasion (3), Bruising (1), Tenderness (2), Contusion (3), Laceration—no sutures (1)	Head (9), Head/Face (1)
(40–50)	3 (5)	Motor Vehicle (3), Assault (1), Fall Standing (2), Motorcycle (1), Fall Moving Object (1)	Abrasion (1), Bruising (1), Tenderness (4), Laceration—no sutures (1), Tenderness (1), Contusion (1), Laceration—with sutures (1)	Head (8)

The first column shows the age at injury as a range. The second column presents the number of genders separately. The rest of the columns indicate the type of injury while the number of patients is noticed within the parenthesis.

By adopting similar methodological modules as in a recent study (Dimitriadis et al., 2018a), we determined a representative source signal for every ROI. The entire procedure is illustrated in **Figure 1b** using an example of time series data obtained from a specific brain region of interest (ROI) (right hemisphere—middle frontal gyrus). In more detail, the contribution of every MEG sensor was weighted by the LCMV beamformer for the reconstruction of a voxel-based time series for the entire predefined grid. The projection of the MEG sensor activity to the source point was performed by means of spatial filters. Each atlas-based ROI contains a different number of voxels. Subsequently, we estimated ROI representative virtual sensors by interpolating functional activity from the voxel time series of individual ROIs (Dimitriadis et al., 2018a). Within each atlas ROI, we estimated the correlation between all possible pairs of source time series in order to map all voxel temporal associations in a common graph (**Figure 1b**, second image from the left). The next step was the calculation of the node-strength of each voxel within the ROI. The strength was determined by summing the connectivity values between a specific node-voxel with the rest of the node-voxels within the same ROI. Then, we normalized the strength values to weights with sum equal to 1 within the ROI. The procedure ended with the estimation of a representative time series for each ROI by summing up across the voxel time series multiplied with their respective weights. This procedure is depicted in **Figure 1b** (upper row, left to right).

Dynamic Functional Connectivity Graphs

In the present study, DFC graphs (DFCG) were calculated separately for each frequency band described previously. The imaginary part of the Phase Locking Value (Dimitriadis et al., 2018a; Palva et al., 2018) or iPLV was used as an FC estimator, a metric that has shown good sensitivity to non-zero-phase lags and tolerability to instantaneous self-interactions from volume conductance (Palva et al., 2018). Given a pair of two phase signals, $\varphi_x(t)$ and $\varphi_y(t)$, derived from the application of the Hilbert transformation to the original signals $x(t)$ and $y(t)$, the iPLV is

described as follows:

$$iPLV_{xy} = \left| \text{im} \left(\sum_t e^{i(\varphi_x(t) - \varphi_y(t))} \right) / N \right| \quad (1)$$

where N is the number of samples and $|\cdot|$ denotes the absolute value operator.

We applied this metric in a dynamic manner for understanding better the time-varying changes of phase-to-phase interactions. This was achieved by computing the iPLV within a series of shifted and overlapping windows, spanning the entire 5-min continuous ROI time series (**Figure 1a**, middle column). The window length of each temporal segment (or timestamp) was set to 2 s with an overlap of 10% for each frequency band. The resulting number of timestamps was equal to 1,785 per frequency band and subject.

DFCG Filtering

Statistical filtering of the DFCGs

A surrogate analysis was performed to evaluate the non-spurious iPLV connections on each sliding window (i.e., timestamp) for every frequency band. The null hypothesis H_0 examines whether the given iPLV coupling belongs to the empirical distribution estimated by the surrogates. We generated ten thousand surrogate time series to test this hypothesis by selecting a random cut-point in the middle of the time series and changing thereafter the order of the two reproduced temporal segments. We repeated the same procedure for each of the 90-source virtual time series (Aru et al., 2015). This procedure ensured similar statistical properties for both original and surrogate iPLV ($iPLV_s$). After estimating the empirical distribution, a statistical level of significance was determined for every iPLV by estimating the amount of $iPLV_s$ that was higher than the original iPLV. The p -value was set to 0.05. A further condition was applied for assessing multiple comparisons within each quasi-static FCG (a 90×90 matrix with tabulated p -values) with the expected fraction of false positives being at the level of 0.01 (Benjamini

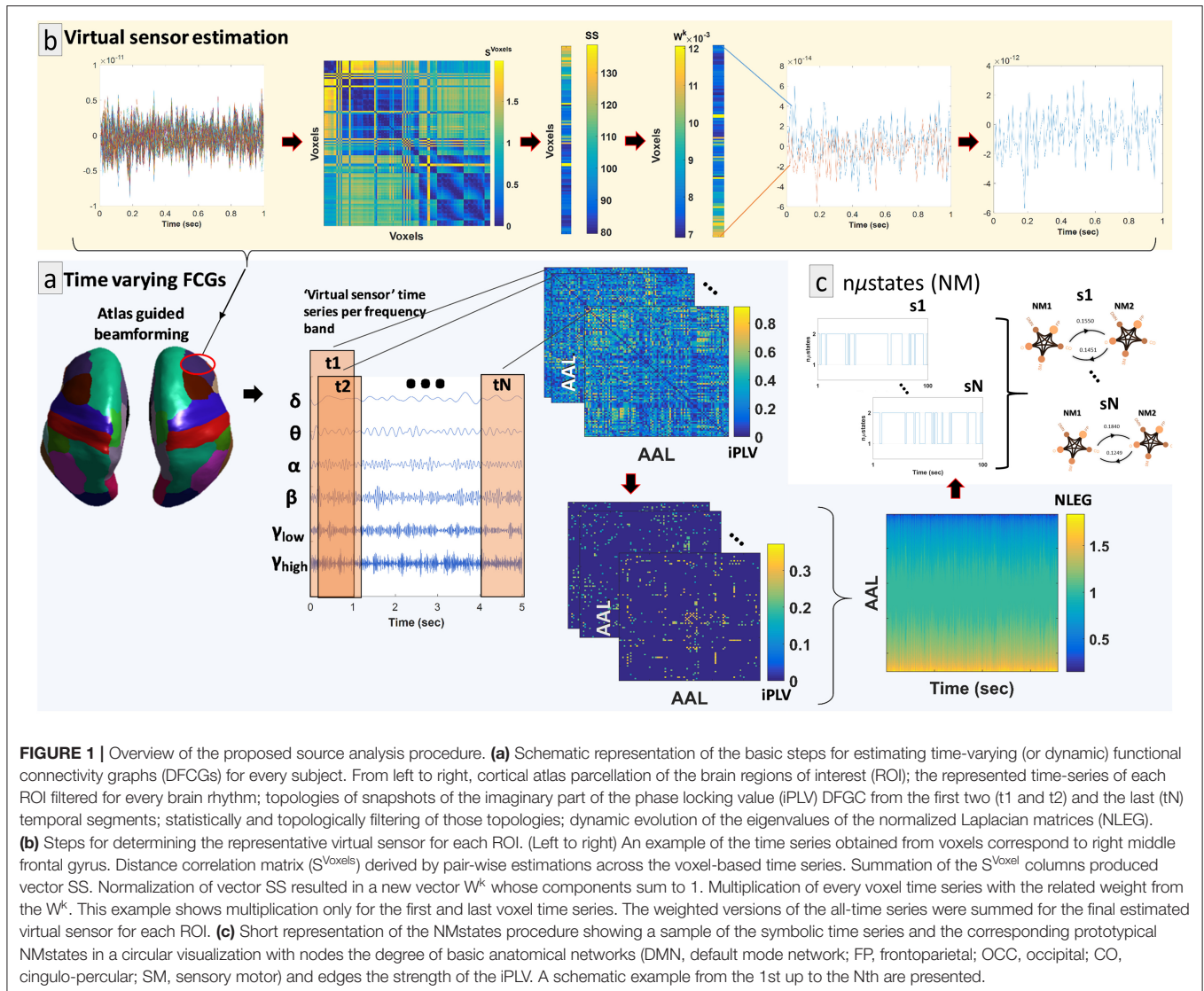


FIGURE 1 | Overview of the proposed source analysis procedure. **(a)** Schematic representation of the basic steps for estimating time-varying (or dynamic) functional connectivity graphs (DFCGs) for every subject. From left to right, cortical atlas parcellation of the brain regions of interest (ROI); the represented time-series of each ROI filtered for every brain rhythm; topologies of snapshots of the imaginary part of the phase locking value (iPLV) DFCG from the first two (t_1 and t_2) and the last (t_N) temporal segments; statistically and topologically filtering of those topologies; dynamic evolution of the eigenvalues of the normalized Laplacian matrices (NLEG). **(b)** Steps for determining the representative virtual sensor for each ROI. (Left to right) An example of the time series obtained from voxels correspond to right middle frontal gyrus. Distance correlation matrix (S^{Voxels}) derived by pair-wise estimations across the voxel-based time series. Summation of the S^{Voxel} columns produced vector SS. Normalization of vector SS resulted in a new vector W^k whose components sum to 1. Multiplication of every voxel time series with the related weight from the W^k . This example shows multiplication only for the first and last voxel time series. The weighted versions of the all-time series were summed for the final estimated virtual sensor for each ROI. **(c)** Short representation of the NMstates procedure showing a sample of the symbolic time series and the corresponding prototypical NMstates in a circular visualization with nodes the degree of basic anatomical networks (DMN, default mode network; FP, frontoparietal; OCC, occipital; CO, cingulo-percular; SM, sensory motor) and edges the strength of the iPLV. A schematic example from the 1st up to the Nth are presented.

and Hochberg, 1995). The non-significant values were set to zero, and the final DFCG had a 3D dimension of 1,785 (segments) \times 90 (sources) \times 90 (sources) per subject and frequency band.

Topological filtering of the DFCGs

In addition to statistical filtering, a data-based topological connection-cutting scheme was applied, based on a recently suggested procedure (Dimitriadis et al., 2017). The so-called Orthogonal Minimal Spanning Trees (OMST¹ was performed to uncover the entire structure of the most dominant paths within every quasi-static FCG (Figure 1a, middle column). The OMST procedure initially emerged from the notion that a fully connected FCG can be reduced to an acyclic FCG or MST of minimum cost from the root node to leaf node without changing the ordered strength of connections (Dimitriadis et al., 2017). Subsequently, the global efficiency of the specific MST was

optimized, preserving the same total cost among the connections (Dimitriadis et al., 2017). The resulting DFC profiles were 3D arrays of size 1,785 (timestamps) \times 90 (sources) \times 90 (sources) for every subject and frequency band.

Symbolization of the DFCG

In this subsection, we briefly introduce our methodological procedure and necessary notations which have been presented in great detail in previous studies (Dimitriadis et al., 2018a). The dynamic connectivity patterns (DFCG) can be transformed into prototypical network microstates (NMstates) based on a vector quantization procedure for effective DFCG modeling (see section Methods in **Supplementary Material**). The input of this procedure was a 2D matrix V . The steps for calculating this matrix are summarized in the following paragraph.

We first calculated the normalized Laplacian matrix (Chung and Graham, 1997) for every quasi-static FCG based on

¹https://github.com/stdimitr/topological_filtering_networks.

the equation,

$$L = I - D^{-\frac{1}{2}} \cdot G \cdot D^{-\frac{1}{2}} \quad (2)$$

where I denotes the identity matrix, D is the degree matrix and G is the quasi-static FCG [90 ROI \times 90 ROI] from every subject and frequency band. Then, eigenvalue analysis ($N_{\text{eigenvalues}} = 90$) on the normalized Laplacian transformations was employed to reveal the synchronization level of the original FCGs (**Figure 1a**, right column). In this form, the richness of information existing in the DFC profiles was represented by a decomposition matrix U that described the assignment of input V to code vectors. In the current work, we used the statistically and topologically filtered DFCs in their inherent format, i.e., as 3D tensors (the third dimension was time). This step derived the 2D matrix V with the first dimension denoting the number of decomposed eigenvalues (90) and the second the number of timestamps (1,785).

Subsequently, we followed a vector quantization process (Dimitriadis et al., 2013) for modeling individual DFC profiles as NMstates (or NM_i for $i = 1, \dots, k$) of a small number k symbols (**Figure 1c**). An approximation for the vector quantization process was obtained by the neural-gas (NG) algorithm (Martinetz et al., 1993). The NG model implements an artificial neural network that converges efficiently to a small number k of codebook vectors with negligible loss of information (see details of the algorithm in section Methods in **Supplementary Material**). A stochastic gradient descent procedure with a softmax adaptation rule minimized the distortion error DE between the original data vector ($v(t) \in V$) and the reconstructed $v_{\text{rec}}(t)$ as follows:

$$DE = \frac{\sum_{t=1}^{N_{\text{total}}} \|v(t) - v_{\text{rec}}(t)\|^2}{\sum_{t=1}^{N_{\text{total}}} \|v(t) - \bar{v}\|^2} \quad (3)$$

$$\text{for } t = 1, \dots, T \text{ and } \bar{v} = \frac{1}{N_{\text{total}}} \sum_{t=1}^{N_{\text{total}}} v(t)$$

where $T = 1,785$ timestamps. The smaller the DE , the better the encoding. This index gets smaller with the increase of k . The total number of the representative symbols was fixed at $k = 2$. For this k , the DE between the original $FC^{\text{L-EIGEN}}$ time series (L: Laplacian - Eigen: Eigenanalysis) and the reconstructed $FC_{\text{rec}}^{\text{L-EIGEN}}$ time series (based on the symbolic time series) was $<2\%$ for every subject and frequency band. The estimated normalized Laplacian-based symbolic times series that preserved the information of NMstates are indicated hereafter as $STS^{\text{L-EIGEN}}$. An $STS^{\text{L-EIGEN}}$ can be viewed as a first-order Markovian chain that describes the temporal evolution of NMstates for every subject.

After computing individual NMstates in every single subject, we estimated the cosine similarity between the $k = 2$ NMstates of every single subject, constructing a similarity matrix of size $[2 \times \text{subjects}] \times [2 \times \text{subjects}]$ independently for each group. Afterwards, we applied K-means clustering in order to organize NMstates within the subjects of every cohort. Based on the silhouette index, the number of clusters was optimal for $k = 2$. At group level, we estimated the cosine similarity between the [2

NMstates \times HC] and [2 NMstates \times mTBI] and, based on the highest cosine value, we aligned NMstates between the 2 groups.

Network Metrics Derived From NMstates and Brain Subnetworks

In every node of the statistically and topologically filtered quasi-static FCG, we calculated the mean degree and strength across the NMstates by employing subject-specific STS. In particular, the degree was defined as the total number of connections in every node resulting in a vector of 90 values per quasi-static graph, brain rhythm, and subject [90 (ROIs) \times 1,785 (temporal segments) \times 6 (frequencies) \times 80 (HC + mTBI subjects)]. Moreover, to better understand the network connectivity in the whole brain, we estimated the mean degree within and between the following five brain anatomical subnetworks (BAN) in pairs, the default mode network (DMN), the sensorimotor (SM), the frontoparietal (FP), the occipital (OCC), and the cingulo-opercular (CO) (these abbreviations were used to present interactions among these brain networks). We followed the same analysis for the estimation of mean functional strength within and between the five brain subnetworks.

First, we summarized the mean degree in every brain region, within and between five subnetworks for every NMstate across frequency bands in both subject groups, for every brain region. A statistical assessment on the mean degree was followed separately for each NMstate, across all six frequency bands and in every brain region, within the five brain subnetworks and among them (overall ten combinations). Mean degree was estimated independently for each subject.

We then adopted a statistical procedure to estimate the significance level for each brain region within and between the five brain subnetworks per frequency band and NMstate. The procedure included a normality control based on the Kolmogorov-Smirnov test and, depending on the outcome, the use of either the parametric pair-wise sample t -test or the non-parametric pair-wise Mann-Whitney u -test (Antonakakis et al., 2016). The significance threshold of the p -value was set to 95% ($p < 0.05$). By adopting the False Discovery Rate (FDR) adjustment (Benjamini and Hochberg, 1995), we corrected the resulting p -values for multiple comparisons.

Temporal Evolution of Modularity Organization of NMstates

To track fluctuations in topological mapping (TM) over time, we followed a novel analysis scheme that did not require labeling of each node into a pre-defined topological mapping class (Shine et al., 2016). For every frequency band and NMstate, we first applied the modularity algorithm to partition each brain network into a number of classes and then we computed the modularity index Q that shows the quality of the partition, the module degree Z -scored, W_τ and the participation coefficient, B_τ , averaged across the network. A joint histogram of within-module (module degree z -scored, W_τ) and between-module (participation coefficient, B_τ) network metrics, named as *topological mapping profile* (Shine et al., 2016), was produced. This profile was calculated for each NMstate for assessing whether the resting brain representation fluctuates over

time between the two network microstates. The first step on calculating the TM was to define the modularity index, which statistic quantifies the degree to which the network may be subdivided into such delineated groups (Rubinov and Sporns, 2010). A fine-tuning algorithm from the Brain Connectivity Toolbox² was used to estimate this statistic for every timestamp, frequency band, and subject. Based on the same toolbox, we then estimated the within-module connectivity by employing the time-resolved module-degree z-score (W_τ ; within module strength) for each region r in our analysis (Shine et al., 2016).

$$W_{r\tau} = \frac{\kappa_{r\tau} - \kappa_{s_r\tau}}{\sigma_{\kappa_{s_r\tau}}} \quad (4)$$

where $\kappa_{s_r\tau}$ is the strength of connections from region r to other regions in its module s_r at time τ , $\kappa_{s_r\tau}$ is the average of κ over all the regions in s_r at time τ , and $\sigma_{\kappa_{s_r\tau}}$ is the standard deviation of κ in s_r at time τ .

The participation coefficient, B_τ , is a metric for the quantification of the extent to which a region connects across all modules (i.e., between-module strength). The B_τ was calculated within each timestamp B_τ for each brain region based on the following equation:

$$B_{r\tau} = 1 - \sum_{s=1}^{n_M} \left(\frac{\kappa_{rs\tau}}{\kappa_{r\tau}} \right)^2 \quad (5)$$

where $\kappa_{rs\tau}$ is the strength of the positive connections of region r to regions in module s at time τ , and $\kappa_{r\tau}$ is the sum of strengths of all positive connections of region r at time τ . The value of $B_{r\tau}$ on a region r is close to 1 or 0 if its connections are uniformly distributed among all the modules or its connections are only within its own module, respectively.

In the final comparison stage we followed two directions, specifically (1) we estimated the relative difference of topological mapping profiles between the two groups for each NMstate and (2) we compared the two NMstates in terms of Q , B_τ and W_τ for every frequency band and group. For the latter comparison, the statistical analysis scheme was the same as described in subsection Network Metrics Derived From NMstates and Brain Subnetworks, where this time the inputs were grouped by NMstate, not by group (HC or mTBI).

Chronnectomics: Characterization of Temporal Dynamics of NMstates

We calculated DFC metrics based on the so-called *chronnectomic* features, which were estimated from the STS^{L-EIGEN} that expressed changes among the NMstates (Dimitriadis et al., 2018b). The first metric was the flexibility index (FI) that expressed the transition rate among the NMstates and was estimated from the following equation,

$$FI = \frac{\text{number of transitions}}{\text{slides} - 1} \quad (6)$$

where *slides* denotes the number of timestamps or temporal segments. FI yields higher values for increased numbers of

brain “hops” between the NMstates. The next metric was the Occupancy Time (OT) that accounts for the percentage of occurrence of an NMstate across the experimental time and is computed as

$$OT(k) = \frac{\text{frequency of Occurance}}{\text{slides}} \quad (7)$$

where *slides* denote the number of timestamps and k denotes the NMstates. Another metric was the complexity index (CI) of an STS^{L-EIGEN}, which was estimated as

$$CI(STS^{L-EIGEN}) = \sum_{l=1}^n c^l(STS^{L-EIGEN}) \quad (8)$$

where $c^l(STS^{L-EIGEN})$ denotes the number of distinct substrings of STS^{L-EIGEN} of length l (Dimitriadis et al., 2013, 2018b; Antonakakis et al., 2016). The parameter l was set to 10 for all frequency bands and subjects. An additional metric was the Dwell Time (DT), which accounts for the time that the brain spends within a particular NMstate before it transitions to another state. In contrast to the OT chronnectomic, DT is the amount of consecutive periods that the brain sticks to a particular state, whereas OT measures the summation of time that the brain spends on a brain state. The last metric used was the Transition Probability Matrix, which accounts for the pairwise transitions of brain states over a common codebook, scanning the Markovian chain from left to right. For example, if the following STS describes the temporal evolution of three brain states [1 2 2 1 2], then the pairwise transitions (PT) are equal to: $PT_{12} = 2/4 = 0.5$ and $PT_{21} = 1/4 = 0.25$. The size of the pairwise transition matrix is equal to (the number of brain states) \times (the number of brain states).

We assessed the level of significance of the aforementioned chronnectomic features by adopting a surrogate data analysis. We shuffled 1,000 times the subject-specific STS^{L-EIGEN} resulting in 1,000 surrogate chronnectomics estimates. Then, we assigned a p -value to every subject-specific chronnectomic metric by comparing the original value with the 1,000 surrogate values. Finally, we analyzed the subject-specific chronnectomic features that were statistically significant ($p < 0.01$) only at group-level. For pairwise transitions, we created a transition matrix by assigning a p -value to each pairwise transition. Subsequently, we controlled for multiple comparisons using FDR, separately in each frequency band.

Classification and Statistical Assessments

We followed an iterative 10-fold cross-validation procedure to assess the performance of NMstates in predicting the class label (HC or mTBI) of the test subjects. The 10-fold cross-validation was repeated one thousand times and, in each iteration, cross-validation was repeated twice, separately for each NMstate (vector of 90 eigenvalues) from the STS^{L-EIGEN} time series. To demonstrate the efficiency of our approach, we adopted the simple k-Nearest Neighbor or k-NN classifier (Horn and Mathias, 1990) with $k = 10$. In every fold, we trained the k-NN classifier with the specific training dataset ([no

²<http://www.brain-connectivity-toolbox.net/>.

of train subjects \times 90 eigenvalues], where the 90 eigenvalues expressed the NMstates) that included data from both groups. We tested its performance on the testing dataset ([no of test subjects \times 90 eigenvalues]). In addition to the previous classification scheme, we further tested the discrimination ability of the chronnectomics in predicting the class label of the test subjects across the frequency bands. In this approach, a rank-feature procedure was used for the selection of the ten most dominant chronnectomics in every fold. For both schemes, we quantified classification performance based on index accuracy (percent of the discrimination level), sensitivity (the portion of the actual mTBI labels), and specificity (the portion of the actual HC labels).

Statistical analysis of the feature vectors employed for classification was used to further confirm the discrimination level between the two groups. The null hypothesis H_0 tested whether the groups contain an equal mean value per feature vector. We examined the H_0 using either a parametric pair-wise sample t -test or a non-parametric pair-wise u -test, based on the outcome of a normality test (Kolmogorov-Smirnov test) on the input data (the statistical steps were the same as the ones described in section Network Metrics Derived From NMstates and Brain Subnetworks). The significance threshold of the p -value was set to 95% ($p < 0.05$), corrected by applying the FDR adjustment.

RESULTS

From Multichannel Recordings to a Restricted Repertoire of Quasi-Static NMstates

Our analytical pipeline revealed unique functional connectivity patterns (NMstates) of phase-synchronized activity that can be considered as discrete brain states: the human brain switches among characteristic NMstates whose temporal evolution can convey important information. The error between the original FC time series and the reconstructed FC time series was $<2\%$ for every subject and frequency band. Our analyses thus showed that two NMstates could describe the temporal evolution of eigenvalues in every subject of both groups and across all frequency bands studied. **Figure 2** shows two examples of state transitions of NMstates, for a control (HC) and an mTBI subject, using activity in the δ frequency band. Modeling the temporal evolution of eigenvalues results in a symbolic time series, indicated by $STS^{L-EIGEN}$ (**Figure 2**) that preserves the temporal information of the characteristic NMstate at every temporal segment. In addition to the representative $STS^{L-EIGEN}$, we considered NMstates as brain topologies with nodes five characteristic brain subnetworks (DMN, SM, FP, OCC, and CO), and as connections the mean degree between brain areas located within those subnetworks.

Figure 3 shows the transitions between two NMstates (NM1 and NM2) for all groups and frequency bands. NMstates are sketched as 5-to-5 networks, where the size and color of a node encode the mean degree within a subnetwork, whereas the color of the between sub-network connections encodes the

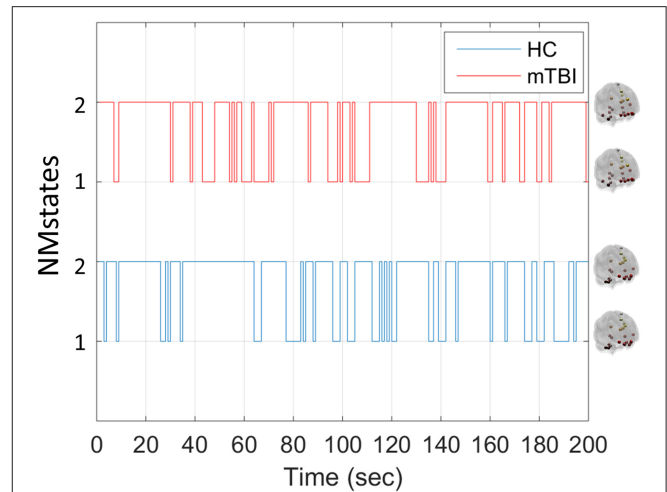


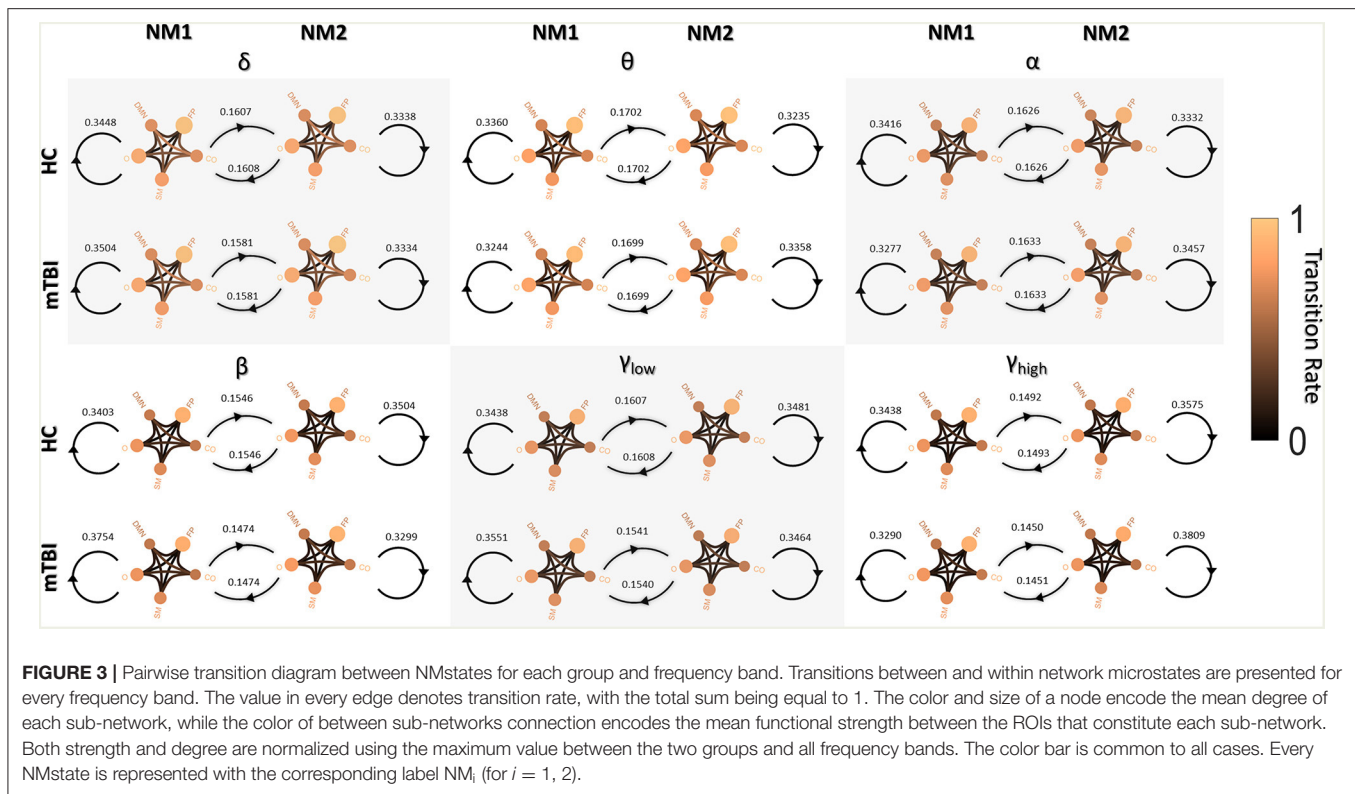
FIGURE 2 | Example of temporal evolution of NMstates for representative HC and mTBI subjects in delta frequency band. Sample symbolic time series for the delta frequency for the HC and mTBI group in order to show how a symbolic time series progresses on time. The brain topologies represent the mean degree of every node that constitutes the default mode network for each NMstate.

functional strength among the ROIs that constitute those subnetworks. A stronger connection occurs between the CO and DMN compared to the other network connections (see DMN—OCC connections in every 5-to-5 network). An overall reduction in averaged strength is observed for all the network connections among the 5-to-5 networks from the lowest frequency band to the highest frequency band. The bidirectional transition rate was higher for the HC group in all the frequency bands apart from α . The self-loop transition rate for the NM1 was higher for the mTBI than the HC in the frequency bands δ , β and γ_{low} and for the HC group in the rest frequency bands. Regarding the self-loop transition rate for the NM2, higher values were observed for the HC in the frequency bands δ , β and γ_{low} and for the mTBI in the rest frequency bands.

Aberrant Higher-Lower Mean Degree for mTBI Subjects

Figures 4, 5 summarize the mean degree for two NMstates (NM1 and NM2) across the frequency bands in both groups and each brain region, within and between the five subnetworks. We found statistically significant differences between the two groups in most within and between brain regions, but no differences were observed on the mean degree of the individual brain regions. A separate statistical group comparison was followed for each NMstate and frequency band. Our analysis revealed an aberrant higher-to-lower pattern of degree reduction for mTBI subjects compared to the HC group.

Then we compared the mean degree between HC and mTBI, only for the cases that survived the FDR adjustment. We started the comparison driven by NMstates and then by frequency bands and we continued with the individual brain regions, the within or between brain subnetworks. The total number of



tested hypotheses (whether mTBI and HC have an equal mean degree) was 1,080 (6 bands \times 2 NMstates \times 90 brain regions) and 180 (6 bands \times 2 NMstates \times 15 BAN combinations). Before FDR correction, there were 138/1,080 and 133/180 p -values smaller than 0.05. No p -values survived for the individual brain regions but 116 (58 per NMstate)/180 p -values survived after FDR correction. In the next paragraph, we describe only the statistical differences occurred in the mean degree of within or between brain subnetworks cases.

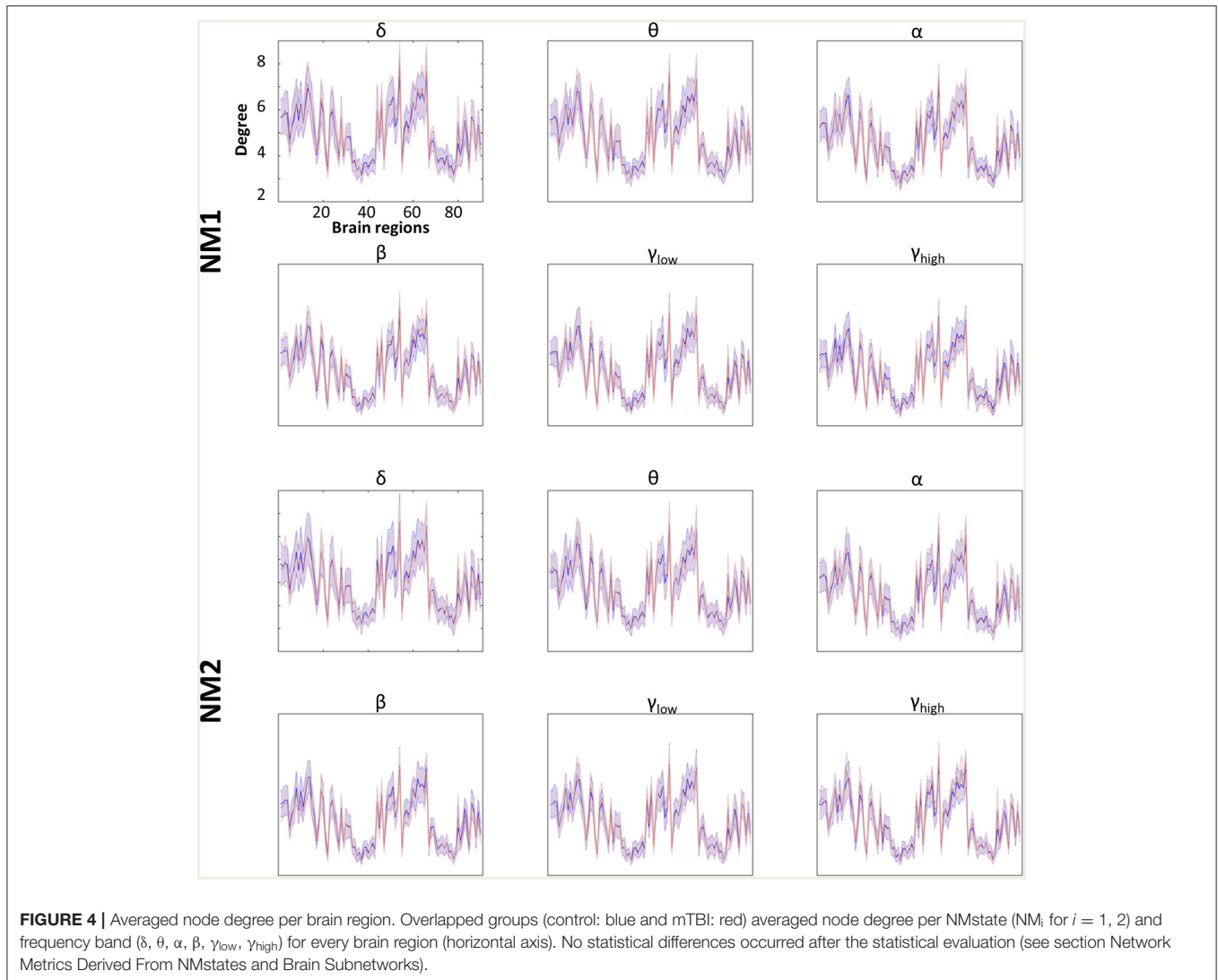
For the NMstate 1 (NM1 in **Figure 5**), the mean degree for HCs was higher in 38 cases (14 within BAN–2 in δ up to β and 3 for the γ_{low} and 3 for the γ_{high} , and 24 between BAN–6 in θ and α , 1 in δ and β , 7 in γ_{high} , and 3 in γ_{low}) whereas the mean degree for mTBI was higher in 20 cases (7 within BAN–3 in δ , 1 in α and γ_{low} , and 2 in β , and 13 between BAN–6 in β , 4 in δ , 2 in α , and 1 in γ_{low}). Furthermore, in all frequency bands, the mean degree within the CO and DMN showed always the highest degree for HC compared to mTBI group, while the mTBI group showed a higher degree within OCC and SM compared to the HC group. The degree between CO-DMN reached the highest value for the HC group compared to the mTBI group, while the mTBI group showed the highest degree in FP-DMN. With regard to the mean degree in NMstate 2 (NM2 in **Figure 5**), the HC degree was higher in 35 cases (15 within BAN–2 in δ up to α and γ_{high} , 4 in γ_{low} and 3 in β , and 20 between BAN–2 in α and γ_{low} , 5 in δ , 3 in θ , 7 in β and 1 in γ_{low}) while mTBI showed higher degree values in 23 cases (6 within BAN–2 in θ and γ_{high} , 1 in α and γ_{low} , and 17 between BAN–2 in θ and γ_{low} ,

6 in α and 7 in γ_{high}). In addition, we observed the same trend in NM2 for within and between BAN for the HC and mTBI groups as in NM1.

Abnormal Fluctuations of Topological Mapping Profile in mTBI

In **Figure 6** we depict the topological mapping (TM) for the frequency band δ (**Figure 6A**) and a comparison on the number of the non-zero bins is shown in its second part (**Figure 6B**). We present this band as an example as similar patterns were observed for the rest of the frequency bands with tiny changes (see section Results in **Supplementary Material**). The TM profiles were higher for the HC than mTBI groups for this specific band in both network microstates (**Figure 6A**, left and middle columns), while the relative difference between the two groups showed more positive values for mTBI compared to the HC, indicating a higher temporal modular stability of the HC compared to the mTBI (**Figure 6A**, right column). This higher entropic profile of temporal modular architecture of mTBI NMstates revealed a new feature for characterizing temporal functional brain networks. This relative difference is illustrated in **Figure 6B** based on the percentage of the non-zero bins of the histogram (see **Figure 6A**). We observed that the sign percentage of the non-bins was substantially higher for the mTBI (>70%–positive) than the HC group (<40% negative) consistent across the frequency bands and NMstates.

In **Figure 7**, we examine whether the average value across all brain regions and subjects per group (HC: upper row and mTBI:

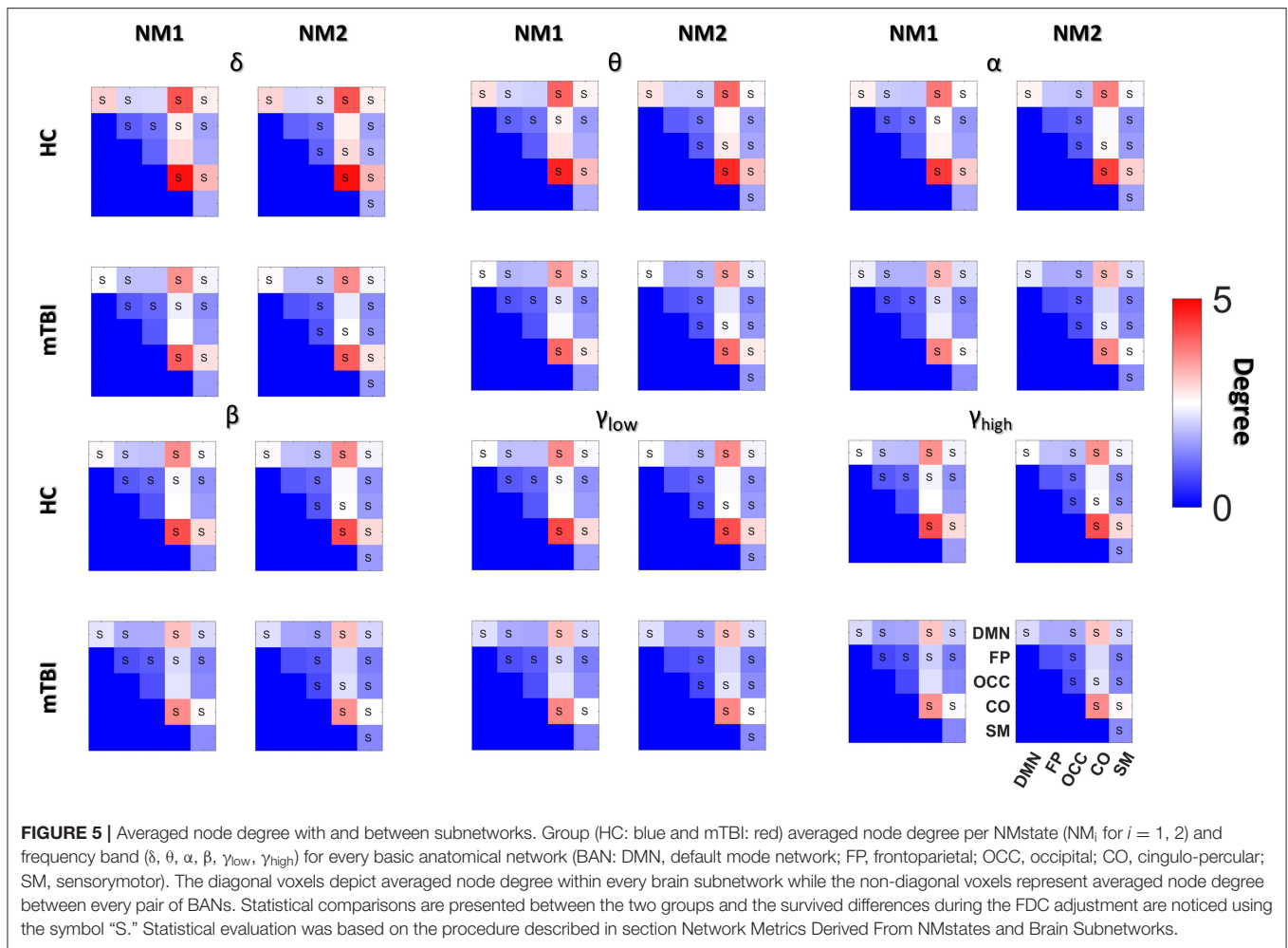


lower row) for every network metric (Q : modularity index, W_τ : module degree Z-scored and B_τ : Participation coefficient) and frequency bands, was significantly different between the networks microstates (NM1 and NM2).

Focusing on Q in both groups (Figure 7, left column), higher values for NM2 than NM1 were estimated for all frequency bands apart from δ and γ_{high} and statistically significant only for the frequency bands θ , α (NM2 > NM1, $p < 0.001$) and γ_{low} (NM2 > NM1, $p < 0.01$). We observed that no significant differences occurred between the NMstates for the network metric W_τ , even though, larger variations occurred between them across all frequency bands and groups (Figure 7, middle column). On the last column of Figure 7, the average value of B_τ across brain regions and subjects is found significantly higher for the NM1 than NM2 in the frequency bands θ , α ($p < 0.001$) for both groups. For γ_{low} , we observed that NM1 was significantly higher than NM2 ($p < 0.05$) for HC group but, for mTBI, we observed the opposite (NM2 > NM1, $p < 0.05$).

Classification Performance With Chronnectomics and NMstates

Table 2 summarizes the results of classification performance (in % for accuracy, sensitivity, and specificity) based on two NMstates (NM1 or NM2) and all chronnectomic features in all the frequency bands. With regard to the ability of the NMstates to discriminate the two groups (Table 2A), high classification performance was observed for both NMstates. In particular, the highest accuracy (>96%) was observed in the α , β , and γ_{low} frequency bands for NM1, while the rest of the cases also showed very high accuracy (>91%). The sensitivity was always 100% but the specificity ranged from 77 to 87%. Table 2B summarizes the classification results obtained using all chronnectomics metrics, namely Flexibility Index (FI), Occupancy Time (OT), and Dwell Time (DW), and the Complexity Index (CI). As can be seen, classification performance was much lower (80%) than in the previous case, showing good sensitivity but very low specificity. Figure 8A shows the group average FI and CI features for



every frequency band, whereas **Figure 8B** depicts OT and DW per NMstate and frequency band. Statistical analysis revealed significant higher FI and DW in NM1 for the HC group compared to the mTBI group in the β frequency band.

DISCUSSION

In the current study, we developed a framework for analyzing the spatiotemporal evolution of functional connectivity patterns of the MEG source-reconstructed activity at rest for mTBI and HC subjects. Each frequency-dependent DFCG was discretized via the neural-gas algorithm into a symbolic time series that described the temporal evolution of brain states (NMstates). DFCGs were treated as first order Markovian chains from which valuable chronnectomic markers were estimated. Our results revealed significantly lower values of the flexibility index (FI) and dwell time (only for the second NMstate) for the mTBI subjects compared to the HC subjects in the beta frequency band. Following a machine learning approach, we were able to discriminate the two groups with an 80% accuracy using the chronnectomics derived from the whole set of frequency bands. In contrast, we obtained a higher

classification performance using two NMstates (vectors of 90 eigenvalues) reaching 94% average accuracy across all frequency bands. The estimated topological mapping profiles (module degree W_T vs. Participation Coefficient B_T), summarizing time-resolved modularity organization of the NMstates, revealed a higher entropy for the mTBI group compared to healthy controls (**Figure 6**), consistently across frequencies and NMstates. This topological mapping profile was spatially concentrated for the HC group, while for mTBI was dispersed across the 2D map and this behavior was quantified by the percentage of positive—negative group difference shown in **Figure 6B**. The proposed analysis procedure proved valuable for characterizing the altered whole-brain transitions of characteristic NMstates in mTBI patients compared to controls.

It is strongly believed that long distance functional connections are mainly maintained between brain areas that communicate in low frequency bands (delta and theta), while local or more short-distant functional connections are mainly observed between brain areas oscillating in the beta and gamma frequencies (von Stein et al., 1999; Thatcher et al., 2008). Specifically, in mTBI studies, Sponheim et al. (2011) reported reduced brain connectivity between specific frontal electrode

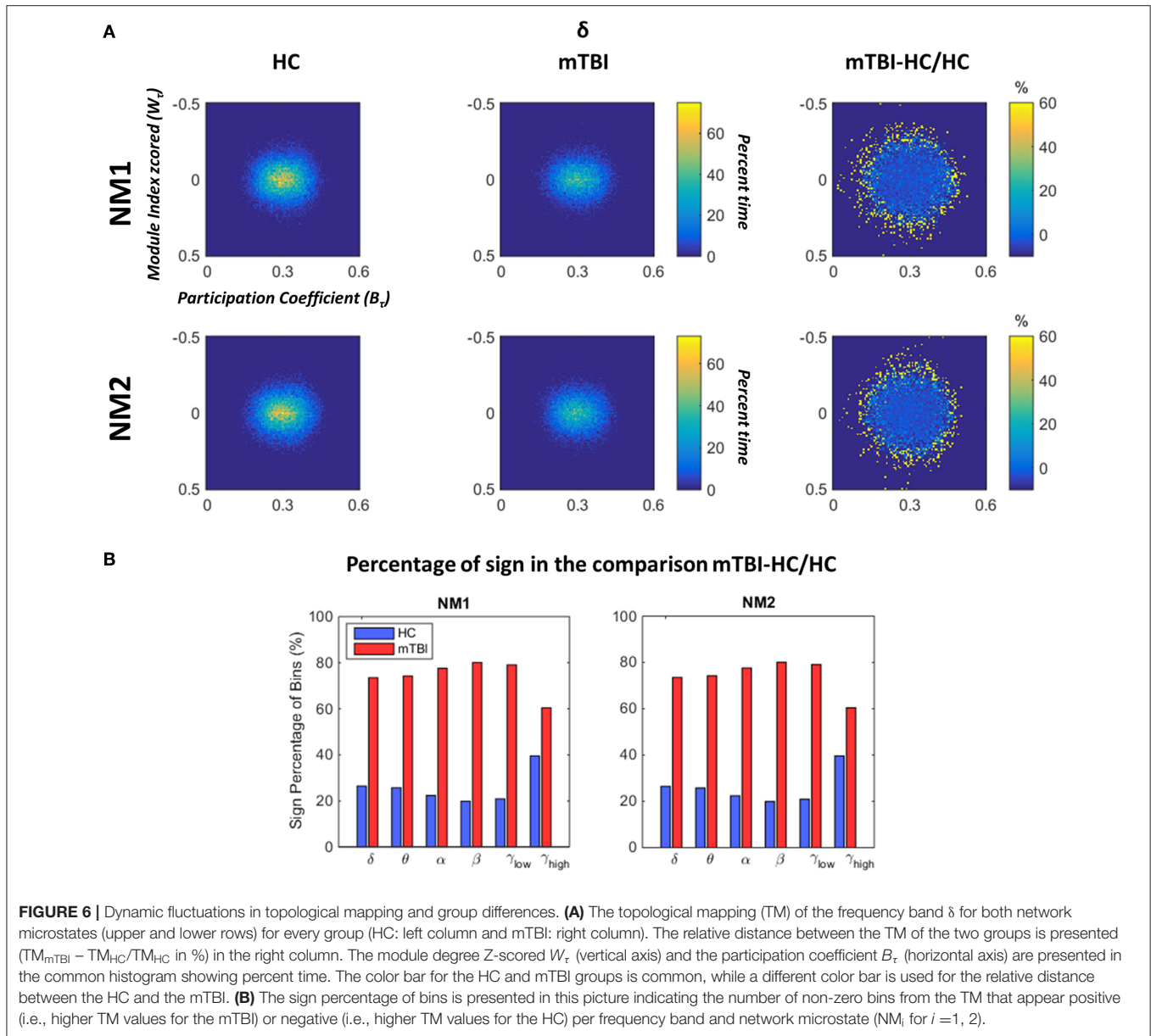


FIGURE 6 | Dynamic fluctuations in topological mapping and group differences. **(A)** The topological mapping (TM) of the frequency band δ for both network microstates (upper and lower rows) for every group (HC: left column and mTBI: right column). The relative distance between the TM of the two groups is presented ($TM_{mTBI} - TM_{HC}/TM_{HC}$ in %) in the right column. The module degree Z-scored W_r (vertical axis) and the participation coefficient B_r (horizontal axis) are presented in the common histogram showing percent time. The color bar for the HC and mTBI groups is common, while a different color bar is used for the relative distance between the HC and the mTBI. **(B)** The sign percentage of bins is presented in this picture indicating the number of non-zero bins in the TM that appear positive (i.e., higher TM values for the mTBI) or negative (i.e., higher TM values for the HC) per frequency band and network microstate (NM_i for $i = 1, 2$).

positions for delta, beta, and gamma frequency bands while Thornton (2003) adopted an audio memory task paradigm and reported that phase and coherence were lowered for the beta1 and beta2 spectral bands (for a review see Rapp et al., 2015). In a follow-up study, they reported an increased connectivity pattern for higher frequencies including alpha, beta frequency and a decreased connectivity pattern for delta, theta brain frequencies (Castellanos et al., 2010). Human beta oscillations (13–30 Hz) are mainly associated with sensorimotor processing (Symons et al., 2016). However, they have been recently linked to attention, emotion, and cognitive control (Guntekin et al., 2013; Symons et al., 2016). Beta frequency is also related to active thinking, focus, high alertness and anxiousness; it is the dominant rhythm in alert or anxious patients.

A recent study in animals and humans, with the support of a biophysical model, tested the theory that beta frequency decrease functions related to sensory or motor information processing in the whole brain (Sherman et al., 2016). They proved that beta is not a byproduct of brain activity but beta signals rather come from the thalamus.

Beta expression and its coherence between distinct brain foci are thought to contribute to information processing at several levels, including communication between neocortical areas (Bressler and Richter, 2015). Sherman’s study provided a unifying link between studies suggesting that beta coordination mediates top-down neocortical processing (Engel and Fries, 2010) and studies showing that top-down influences are communicated through supragranular layers (Rockland and Pandya, 1979).

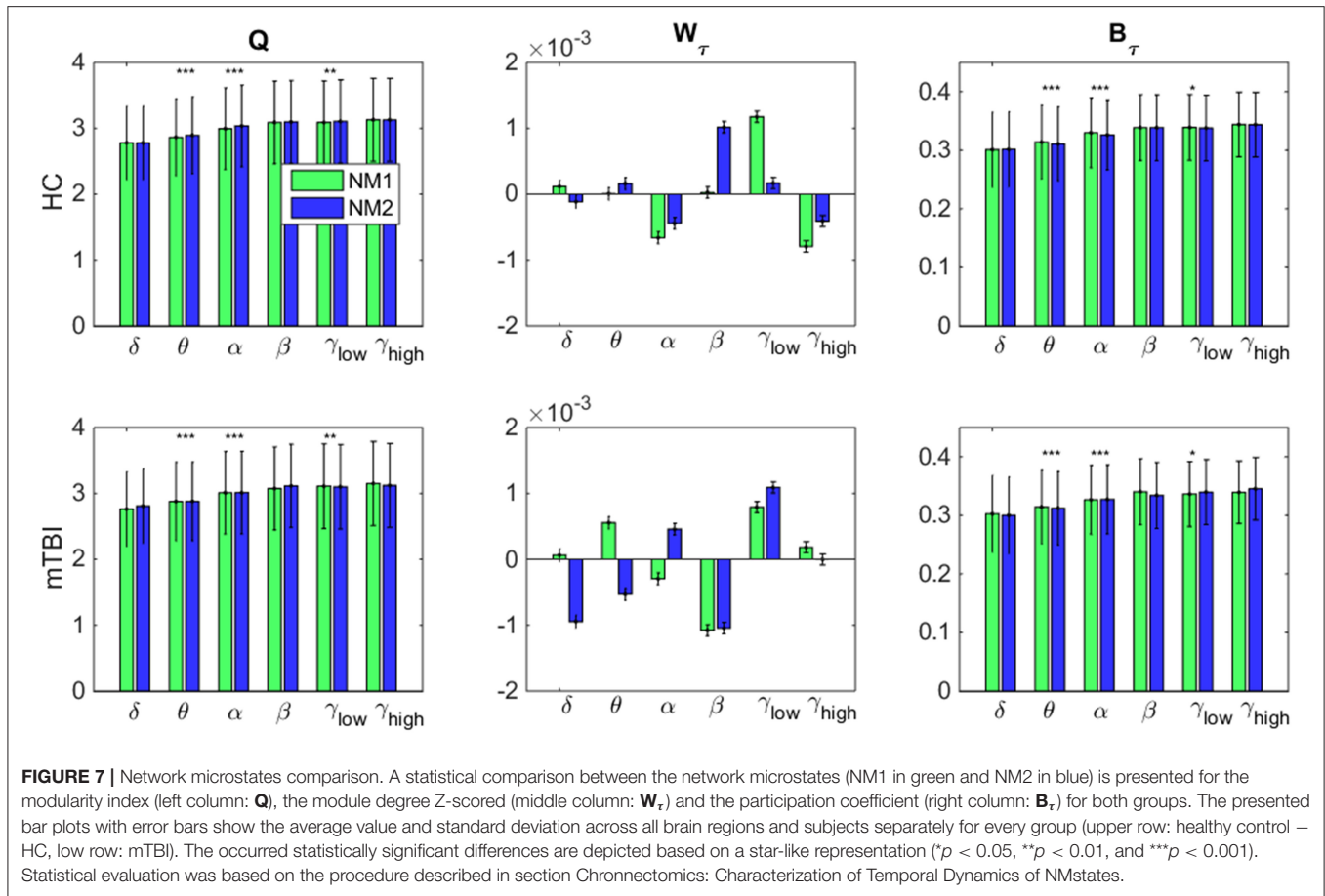


FIGURE 7 | Network microstates comparison. A statistical comparison between the network microstates (NM1 in green and NM2 in blue) is presented for the modularity index (left column: **Q**), the module degree Z-scored (middle column: **W_τ**) and the participation coefficient (right column: **B_τ**) for both groups. The presented bar plots with error bars show the average value and standard deviation across all brain regions and subjects separately for every group (upper row: healthy control – HC, low row: mTBI). The occurred statistically significant differences are depicted based on a star-like representation (**p* < 0.05, ***p* < 0.01, and ****p* < 0.001). Statistical evaluation was based on the procedure described in section Chronnectomics: Characterization of Temporal Dynamics of NMstates.

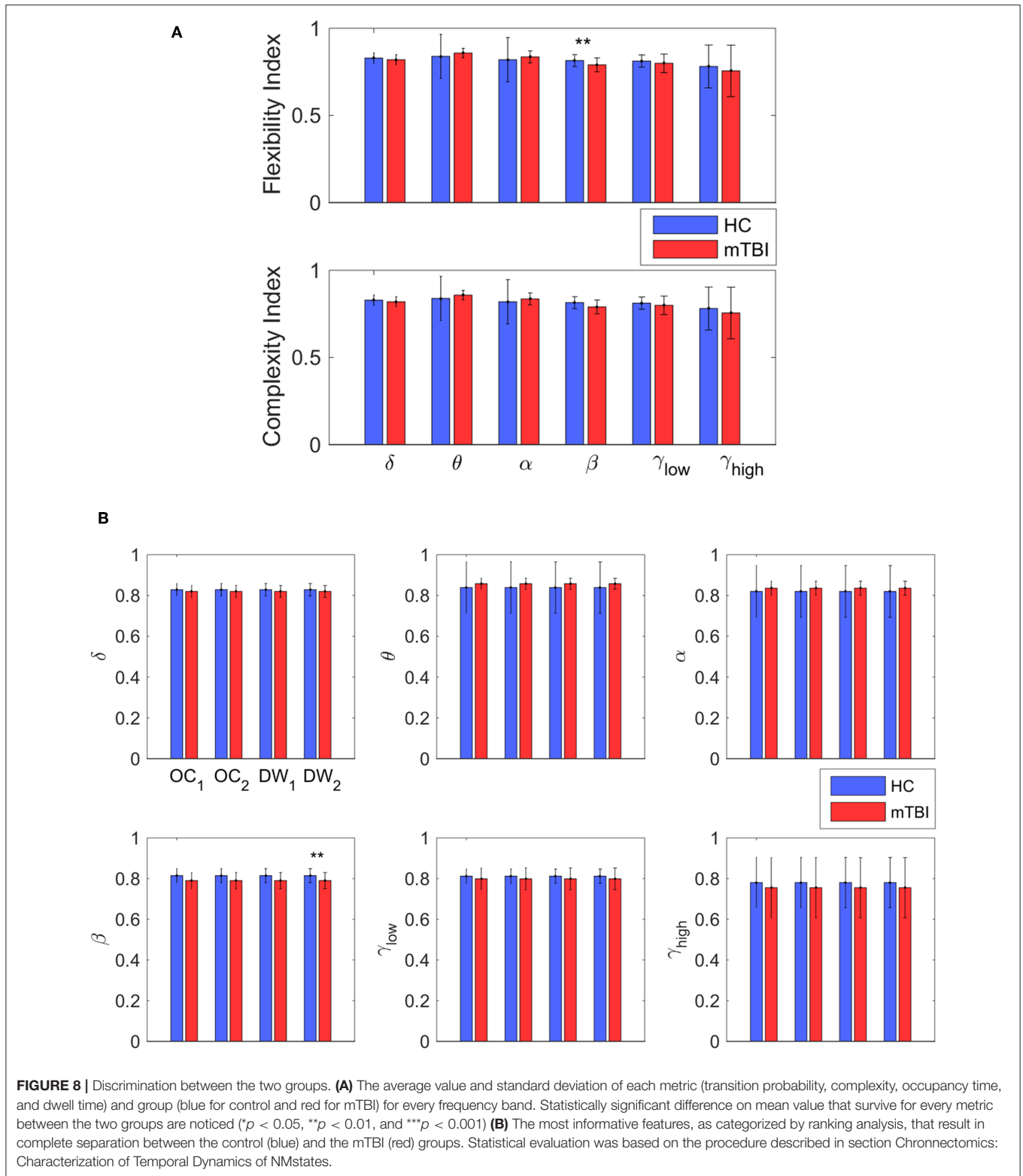
TABLE 2 | Summary of the classification performance (Accuracy, Sensitivity, and Specificity in %) **(A)** per frequency band for every NMstate (NM1 or NM2), and **(B)** including all chronnectomics (Flexibility Index, Occupancy Time, and Dwell Time) and Complexity Index (CI) for all the frequency bands.

NMstates	Frequency band	Accuracy (%)	Sensitivity (%)	Specificity (%)
A				
NM1	δ	91.27 ± 1.34	100	77.30 ± 3.49
	θ	92.27 ± 1.35	100	80.00 ± 3.49
	α	96.14 ± 0.55	100	90.00 ± 1.42
	β	97.42 ± 0.67	100	93.33 ± 1.74
	γ _{low}	93.85 ± 1.22	100	83.97 ± 3.18
	γ _{high}	96.15 ± 0.65	100	90.00 ± 1.68
NM2	δ	93.56 ± 0.73	100	83.33 ± 1.87
	θ	94.85 ± 0.69	100	86.67 ± 1.83
	α	93.84 ± 0.70	100	83.97 ± 1.88
	β	92.88 ± 0.98	100	81.40 ± 2.53
	γ _{low}	93.85 ± 1.22	100	83.97 ± 3.18
	γ _{high}	95.16 ± 0.54	100	87.40 ± 1.39
B				
Chronnectomics + CI		80.34 ± 1.34	99.65 ± 0.32	49.23 ± 3.56

Taking all together, these studies and others suggest that beta frequencies inhibit information processing and decrease focally to allow optimal information relay.

The previous results confirmed three predicted hypotheses—mechanisms where neocortical beta burst events would possibly decrease information relay. The first states that the inputs creating beta may stimulate inhibitory neurons in the top layers of the cortex. The second is devoted to a possible saturation of the activity of pyramidal neurons which, as a consequence, reduce their ability to process information. The third argues that the thalamic bursts producing beta cover the majority of the thalamus, so that it cannot pass information to the cortex. In close analogy to neocortical beta states is the decreased relay of bottom-up motor or sensory information via the thalamus during thalamic alpha states. Possible mechanisms that support this sensory relay during alpha frequency are the following: thalamic hyperpolarization, synaptic depression at thalamocortical synapses, and low capacity for novel external information relay during the co-occurrence of internally generated alpha rhythms in conjunction to beta states (Klimesch, 2012). Our findings in beta frequency with internal co-occurrence of alpha states in relation to the aforementioned hypotheses support a central role of the thalamus impairment in mTBI (Grossman and Inglese, 2016). Sensorimotor driven paradigms applied to mTBI subjects could shed light and further enhance the interpretation of our findings and Sherman’s hypotheses for the mechanisms producing neocortical beta rhythms.

Recent advances in MEG and network neuroscience have shown that mTBI can be manifested as an excessive pattern



of slow-wave activity (Huang et al., 2012), while localization of this slow-wave activity can reveal the foci of the damage (Huang et al., 2014). Dimitriadis et al. (2015) employed PLV to quantify time-static FCGs at the sensor level. They revealed

a dense local and sparse long-range connectivity pattern for healthy controls and a sparse local and dense long-range pattern for the mTBI subjects. Activity in the alpha frequency band was the most discriminative feature for separating the two groups. In

our previous studies (Antonakakis et al., 2015, 2016, 2017a), we combined intra- and inter- frequency couplings in a single FCG, showing a dense network of stronger local and global connections for HC group, in agreement with other studies (Rapp et al., 2015). In our most recent study (Antonakakis et al., 2017b), the mTBI group showed hyper-synchronization in a rich-club network organization compared to the HC group.

Structural neuroimaging combined with diffusion tensor imaging (DTI) has revealed an association of mTBI with aberrant white matter microstructures (Huang et al., 2009). Specifically, a connection was shown between focal increased slow wave activity and the location of white matter injury, which was consistent with the hypothesis that the deceleration of oscillations could be caused by differentiation (Llinás et al., 1999).

A disrupted inter-regional frequency-dependent functional connectivity pattern has also been reported in combat-related blast injury using EEG (Sponheim et al., 2011). Oscillatory functional synchronization between brain areas play a pivotal role in network connectivity and support both cognition and behavior (Ward, 2003; Uhlhaas et al., 2009). The expression of this network connectivity in various frequencies at resting-state is related to the intrinsic multi-frequency organization of brain activity that is pertinent to healthy brain function and dysfunction in various clinical populations (Engel et al., 2014).

The present study explored for the very first time the consequences of mTBI in human brain functionality at resting-state using MEG and DFCG analysis. Our analysis summarized DFCGs with connectivity graphs, where each graph was associated with one NMstate (Functional Connectivity microstate or alternatively brain state). The major outcome of this analysis was a symbolic time series for the temporal description of the evolution of these brain states. Dynamic functional connectivity graphs were treated as Markovian chains from which a variety of chronnectomic metrics were extracted. Recent studies defined microstates in MEG and fMRI modalities using a Hidden Markovian Modeling (HMM) approach employing the band-limited amplitude envelope of virtual source time series (Baker et al., 2014) and the BOLD time series, respectively (Vidaurre et al., 2016). Both methodologies defined microstates in a full analogy to original EEG microstates, via a mining procedure of brain activity rather than the dynamic functional connectivity. Machine learning analysis over the derived chronnectomics produced a high classification accuracy (94%) between healthy controls and mTBI subjects using the NMstates, and an 80% performance when employing chronnectomics across frequencies (Table 2). Compared to the 92% accuracy reported by other studies (Vergara et al., 2018), we reached a slightly higher discrimination between the two groups benefiting from the dynamic content of the network analysis.

Functional MRI (fMRI) studies at resting-state have revealed numerous discrete functional neural networks (De Luca et al., 2005; Damoiseaux et al., 2006). These neural networks include well-described motor, sensory, language, and visual networks (Cordes et al., 2000). In addition, the set of characteristic neural networks comprise brain areas that engage various higher-order cognitive operations that are impaired in TBI-like FP and CO

brain subnetworks (Beckmann et al., 2005; Dosenbach et al., 2007; Seeley et al., 2007). The vast majority of the resting brain's resources (~80%) is expended to maintain the homeostasis between the resting-state networks (Raichle and Mintun, 2006). This observation suggests that resting-state networks are excellent indicators of disruptions of coordinated functional connectivity between brain areas in many disorders and diseases, including mTBI. Researchers have shown a particular interest in the "default mode" network, which is a group of interconnected midline cortical regions that show high activity in the absence of externally-imposed cognitive processing (Buckner et al., 2008). The DMN reduces its activity during cognitive demands and may be involved in self-referential processing and internal emotional states (Power et al., 2011; Barch, 2013). Finally, CO plays a central role in sustaining alertness and attention (Coste and Kleinschmidt, 2016).

Figure 5 demonstrates the global mean degree of the within or between brain region subnetworks for every NMstate across frequency bands in both groups. Our statistical analysis applied independently to every NMstate revealed significant differences between the two groups in most cases. Our analysis revealed an aberrant higher-lower pattern for mTBI subjects compared to healthy controls. The central brain networks that were more connected with the rest of the brain were the CO and DMN across all frequency bands. In mTBI patients, DMN and CO were less connected with the rest of brain networks compared to healthy controls while the degree between CO-DMN was the highest for HC compared to the mTBI while mTBI group showed the highest degree in FP-DMN across all frequency bands (Figure 5). Our results provided the interesting finding that CO and DMN were more central hubs in HC compared to mTBI while CO-DMN were better interconnected also in HC. These findings revealed that attention, sustaining alertness, and other cognitive functions like thinking of others or themselves, remembering the past and planning of the future, that are linked to CO and DMN (Buckner et al., 2008) are impaired in mTBI. This is the very first study that revealed such interesting findings, linking the consequences of mTBI with neuromagnetic whole-brain resting-state networks under the notion of dynamic functional connectivity on the source level. Furthermore, our analysis demonstrated a high classification performance which further enhanced the significance of the proposed procedure. Our study employed beamformed source-reconstruction of resting-state MEG activity in various frequency bands with a common MRI template for all subjects. However, a recent study explored the deviation in power and connectivity of virtual source MEG activity when using a template instead of native MRIs (Douw et al., 2017) and found that relative power, connectivity measures, and network estimates were consistent in both cases.

Figure 6 showed that the time-resolved FCD of the mTBI group are more randomly organized in time compared to the HC group. This is a major result indicating that the specific brain insult may lead to an uncertain network organization over time. However, the present result needs further validation from different mTBI cohorts in order to confirm the temporal instability of the time-resolved network alterations.

With regard to the limitations of the present study, a possible criticism might be the absence of individual MRI data, which potentially could result in more precise source reconstructions. Furthermore, no clinical scores were available for the mTBI group and, therefore, a statistical comparison with the results of the present study was not feasible. Finally, it is worth mentioning that the connectivity metric used did not consider directionality, i.e., the direction of information flow between two interconnected nodes, and the interdependency between frequency bands, as it was presented in our previous study (Antonakakis et al., 2017b). For this purpose, we will conduct a future study to alleviate this limitation.

CONCLUSIONS

In the present study, we examined for the very first time how mTBI affects the dynamics of functional brain networks on beamformed source-reconstructed resting-state activity. Dynamic functional graphs were treated as Markovian chains via a well-established analytic framework that discretized their temporal evolution into a symbolic time series. Symbolic dynamics and chronnectomics have already proven valuable in the discrimination of healthy controls from mTBI subjects. We further propose that network microstates (NMstates) form a valuable connectomic biomarker for detecting mTBI succeeding an average performance of 94% across frequencies. Cingulo-Opercular (CO) and Default Mode Network (DMN) were the central network hubs of the derived brain states (NMstates), where mTBI subjects were less connected with the rest of the brain networks and showed substantially smaller time-resolved organization compared to healthy controls. mTBI subjects showed a higher entropic temporal evolution of modular organization compared to healthy controls. A significant difference on the flexibility index was observed between the two groups for the β frequency band which may support a central role of the thalamus impairment in mTBI. Finally, in a future study, it would be interesting to evaluate the sensitivity of the current analysis approach and chronnectomic features in detecting the return of mTBI subjects back to normal.

DATA AVAILABILITY STATEMENT

The datasets generated for this study will not be made publicly available in accordance with the consent form signed by the subjects. However, requests to see the raw data can be sent to the corresponding author.

REFERENCES

Alhourani, A., Wozny, T. A., Krishnaswamy, D., Pathak, S., Walls, S. A., Ghuman, A. S., et al. (2016). Magnetoencephalography-based identification of functional connectivity network disruption following mild traumatic brain injury. *J. Neurophysiol.* 116, 1840–1847. doi: 10.1152/jn.00513.2016

ETHICS STATEMENT

The studies involving human participants were reviewed and approved by the Institutional Review Board (IRB) and the Human Research Protection Official Review, Department of Defense. The patients/participants provided their written informed consent to participate in this study.

AUTHOR CONTRIBUTIONS

SD conceptualized the research analysis with regard to source connectivity, the connectivity metrics, and the classification scheme. MA contributed to the design of data preprocessing, the statistical assessments, and performed all analyses. In collaboration with SD, MA prepared the figures and drafted the manuscript. AP designed the original study and GZ contributed to the collection of the data and preprocessing methods. MZ, AP, and GZ provided the input on the development of and critique on the revisions of the manuscript. All authors read and approved the final version of the manuscript.

FUNDING

The Department of Defense Congressionally Directed Medical Research Program W81XWH-08-2-0135 has supported the current work. This study was part of the project Integrated Clinical Protocol, conducted by the Investigators and staff of The Mission Connect Mild Traumatic Brain Injury Translational Research Consortium. SD was supported by MRC grant MR/K004360/1 (Behavioral and Neurophysiological Effects of Schizophrenia Risk Genes: A Multi-locus, Pathway Based Approach) and by a MARIE-CURIE COFUND EU-UK Research Fellowship.

ACKNOWLEDGMENTS

We would like to acknowledge RCUK of Cardiff University and the Wellcome Trust for covering the publication fee. This manuscript has been released as a Pre-Print at the bioRxiv (Antonakakis et al., 2019)³.

SUPPLEMENTARY MATERIAL

The Supplementary Material for this article can be found online at: <https://www.frontiersin.org/articles/10.3389/fncom.2019.00090/full#supplementary-material>

³<https://www.biorxiv.org/content/10.1101/596155v1>.

Allen, E. A., Damaraju, E., Plis, S. M., Erhardt, E. B., Eichele, T., and Calhoun, V. D. (2012). Tracking whole-brain connectivity dynamics in the resting state. *Cereb. Cortex* 24, 663–676. doi: 10.1093/cercor/bhs352

Antonakakis, M., Dimitriadis, S. I., Zervakis, M., Micheloyannis, S., Rezaie, R., Babajani-Feremi, A., et al. (2016). Altered cross-frequency coupling in resting-state MEG after mild traumatic brain injury. *Int. J. Psychophysiol.* 102, 1–11. doi: 10.1016/j.ijpsycho.2016.02.002

- Antonakakis, M., Dimitriadis, S. I., Zervakis, M., Papanicolaou, A. C., and Zouridakis, G. (2017a). Altered rich-club and frequency-dependent subnetwork organization in mild traumatic brain injury: a MEG resting-state study. *Front. Hum. Neurosci.* 11:416. doi: 10.3389/fnhum.2017.00416
- Antonakakis, M., Dimitriadis, S. I., Zervakis, M., Papanicolaou, A. C., and Zouridakis, G. (2017b). Reconfiguration of dominant coupling modes in mild traumatic brain injury mediated by δ -band activity: a resting state MEG study. *Neuroscience* 356, 275–286. doi: 10.1016/j.neuroscience.2017.05.032
- Antonakakis, M., Dimitriadis, S. I., Zervakis, M., Papanicolaou, A. C., and Zouridakis, G. (2019). Alterations in dynamic spontaneous network microstates in mild traumatic brain injury: a MEG beamformed dynamic connectivity analysis. *BioRxiv*. doi: 10.1101/596155
- Antonakakis, M., Dimitriadis, S. I., Zervakis, M., Rezaie, R., Babajani-Feremi, A., Micheloyannis, S., et al. (2015). Comparison of brain network models using cross-frequency coupling and attack strategies. *Conf. Proc. IEEE. Eng. Med. Biol. Soc.* 2015, 7426–7429. doi: 10.1109/EMBC.2015.7320108
- Aru, J., Priesemann, V., Wibral, M., Lana, L., Pipa, G., Singer, W., et al. (2015). Untangling cross-frequency coupling in neuroscience. *Curr. Opin. Neurobiol.* 31, 51–61. doi: 10.1016/j.conb.2014.08.002
- Assistant Secretary, D. O. D. (2007). *Traumatic Brain Injury: Definition and Reporting*. Department of Defense. Available online at: https://dod.defense.gov/News/Special-Reports/0315_tbi/
- Baillet, S. (2017). Magnetoencephalography for brain electrophysiology and imaging. *Nat. Neurosci.* 20, 327–339. doi: 10.1038/nn.4504
- Baker, A. P., Brookes, M. J., Rezek, I. A., Smith, S. M., Behrens, T., Probert Smith, P. J., et al. (2014). Fast transient networks in spontaneous human brain activity. *eLife* 3:e01867. doi: 10.7554/eLife.01867.014
- Barch, D. M. (2013). Brain network interactions in health and disease. *Trends Cogn. Sci.* 17, 603–605. doi: 10.1016/j.tics.2013.09.004
- Beckmann, C. F., DeLuca, M., and Devlin, J. T., and Smith, S. M. (2005). Investigations into resting-state connectivity using independent component analysis. *Philos. Trans. R. Soc. Lond. Biol. Sci.* 360, 1001–1013. doi: 10.1098/rstb.2005.1634
- Benjamini, Y., and Hochberg, Y. (1995). Controlling the false discovery rate: a practical and powerful approach to multiple testing. *J. R. Stat. Soc.* 57, 289–300. doi: 10.1111/j.2517-6161.1995.tb02031.x
- Bharath, R. D., Chaitanya, G., Panda, R., Raghavendra, K., Sinha, S., Sahoo, A., et al. (2016). Reduced small world brain connectivity in probands with a family history of epilepsy. *Eur. J. Neurol.* 23, 1729–1737. doi: 10.1111/ene.13104
- Bressler, S. L., and Richter, C. G. (2015). Interareal oscillatory synchronization in top-down neocortical processing. *Curr. Opin. Neurobiol.* 31, 62–66. doi: 10.1016/j.conb.2014.08.010
- Brookes, M. J., Hale, J. R., Zumer, J. M., Stevenson, C. M., Francis, S. T., Barnes, G. R., et al. (2011a). Measuring functional connectivity using MEG: methodology and comparison with fMRI. *Neuroimage* 56, 1082–1104. doi: 10.1016/j.neuroimage.2011.02.054
- Brookes, M. J., Woolrich, M., Luckhoo, H., Price, D., Hale, J. R., Stephenson, M. C., et al. (2011b). Investigating the electrophysiological basis of resting state networks using magnetoencephalography. *Proc. Natl. Acad. Sci. U.S.A.* 108, 16783–16788. doi: 10.1073/pnas.1112685108
- Buckner, R. L., Andrews-Hanna, J. R., and Schacter, D. L. (2008). The brain's default network. Anatomy, function, and relevance to disease. *Ann. N. Y. Acad. Sci.* 1124, 1–38. doi: 10.1196/annals.1440.011
- Calhoun, V. D., and Adali, T. (2016). Time-varying brain connectivity in fMRI data: whole-brain data-driven approaches for capturing and characterizing dynamic states. *IEEE Signal. Process. Mag.* 33, 52–66. doi: 10.1109/MSP.2015.2478915
- Castellanos, N. P., Paúl, N., Ordóñez, V. E., Demuyck, O., Bajo, R., Campo, P., et al. (2010). Reorganization of functional connectivity as a correlate of cognitive recovery in acquired brain injury. *Brain* 133, 2365–2381. doi: 10.1093/brain/awq174
- Chung, F. R. K., and Graham, F. C. (1997). “Spectral graph theory,” in *CBMS Conference on Recent Advances in Spectral Graph Theory and Conference Board of the Mathematical Sciences* (American Mathematical Society). Available online at: <https://www.ams.org/books/cbms/092/>
- Cordes, D., Haughton, V. M., Arfanakis, K., Wendt, G. J., Turski, P. A., Moritz, C. H., et al. (2000). Mapping functionally related regions of brain with functional connectivity MR imaging. *Am. J. Neuroradiol.* 21, 1636–1644. Available online at: <http://www.ajnr.org/content/21/9/1636>
- Coste, C. P., and Kleinschmidt, A. (2016). Cingulo-opercular network activity maintains alertness. *Neuroimage* 128, 264–272. doi: 10.1016/j.neuroimage.2016.01.026
- Da Costa, L., Robertson, A., Bethune, A., MacDonald, M. J., Shek, P. N., Taylor, M. J., et al. (2015). Delayed and disorganized brain activation detected with magnetoencephalography after mild traumatic brain injury. *J. Neurol. Neurosurg. Psychiatry* 86, 1008–1015. doi: 10.1136/jnnp-2014-308571
- Damoiseaux, J. S., Rombouts, S. A., Barkhof, F., Scheltens, P., Stam, C. J., Smith, S. M., et al. (2006). Consistent resting-state networks across healthy subjects. *Proc. Natl. Acad. Sci. U.S.A.* 103, 13848–13853. doi: 10.1073/pnas.0601417103
- De Luca, M., Smith, S. M., De Stefano, N., and Federico, A., and Matthews, P. M. (2005). Blood oxygenation level dependent contrast resting state networks are relevant to functional activity in the neocortical sensorimotor system. *Exp. Brain Res.* 167, 587–594. doi: 10.1007/s00221-005-0059-1
- De Monte, V. E., Geffen, G. M., and Massavelli, B. M. (2006). The effects of posttraumatic amnesia on information processing following mild traumatic brain injury. *Brain Injury* 20, 1345–1354. doi: 10.1080/02699050601082073
- Delorme, A., and Makeig, S. (2004). EEGLAB: an open source toolbox for analysis of single-trial EEG dynamics including independent component analysis. *J. Neurosci. Methods* 134, 9–21. doi: 10.1016/j.jneumeth.2003.10.009
- Dimitriadis, S. I., Antonakakis, M., Simos, P., Fletcher, J. M., and Papanicolaou, A. C. (2017). Data-driven topological filtering based on orthogonal minimal spanning trees: application to multi-group MEG resting-state connectivity. *Brain Connect.* 7, 661–670. doi: 10.1089/brain.2017.0512
- Dimitriadis, S. I., Laskaris, N. A., Simos, P. G., Fletcher, J. M., and Papanicolaou, A. C. (2016). Greater repertoire and temporal variability of cross-frequency coupling (CFC) modes in resting-state neuromagnetic recordings among children with reading difficulties. *Front. Hum. Neurosci.* 10:163. doi: 10.3389/fnhum.2016.00163
- Dimitriadis, S. I., Laskaris, N. A., and Tzelepi, A. (2013). On the quantization of time-varying phase synchrony patterns into distinct functional connectivity microstates (FC μ states) in a multi-trial visual ERP paradigm. *Brain Topogr.* 26, 397–409. doi: 10.1007/s10548-013-0276-z
- Dimitriadis, S. I., López, M. E., Bruna, R., Cuesta, P., Marcos, A., Maestú, F., et al. (2018b). How to build a functional connectomic biomarker for mild cognitive impairment from source reconstructed MEG resting-state activity: the combination of ROI representation and connectivity estimator matters. *Front. Neurosci.* 12:306. doi: 10.3389/fnins.2018.00306
- Dimitriadis, S. I., Routley, B., Linden, D. E., and Singh, D. S. (2018a). Reliability of static and dynamic network metrics in the resting-state: a MEG-beamformed connectivity analysis. *Front. Neurosci.* 12:506. doi: 10.1101/358192
- Dimitriadis, S. I., Zouridakis, G., Rezaie, R., Babajani-Feremi, A., and Papanicolaou, A. C. (2015). Functional connectivity changes detected with magnetoencephalography after mild traumatic brain injury. *Neuroimage* 9, 519–531. doi: 10.1016/j.nicl.2015.09.011
- Dosenbach, N. U., Fair, D. A., Miezin, F. M., Cohen, A. L., Wenger, K. K., Dosenbach, R. A., et al. (2007). Distinct brain networks for adaptive and stable task control in humans. *Proc. Natl. Acad. Sci. U.S.A.* 104, 11073–11078. doi: 10.1073/pnas.0704320104
- Dou, L., Nieboer, D., Stam, C. J., Tewarie, P., and Hillebrand, A. (2017). Consistency of magnetoencephalographic functional connectivity and network reconstruction using a template versus native MRI for co-registration. *Hum. Brain Mapp.* 39, 104–119. doi: 10.1002/hbm.23827
- Dunkley, B. T., Da Costa, L., Bethune, A., Jetly, R., Pang, E. W., Taylor, M. J., et al. (2015). Low-frequency connectivity is associated with mild traumatic brain injury. *Neuroimage Clin.* 7, 611–621. doi: 10.1016/j.nicl.2015.02.020
- Dunkley, B. T., Urban, K., Da Costa, L., Wong, S. M., Pang, E. W., and Taylor, M. J. (2018). Default mode network oscillatory coupling is increased following concussion. *Front. Neurol.* 9:280. doi: 10.3389/fneur.2018.00280
- Eierud, C., Craddock, R. C., Fletcher, S., Aulakh, M., King-Casas, B., Kuehl, D., et al. (2014). Neuroimaging after mild traumatic brain injury: review and meta-analysis. *Neuroimage Clin.* 4, 283–294. doi: 10.1016/j.nicl.2013.12.009
- Engel, A. K., and Fries, P. (2010). Beta-band oscillations—signalling the status quo? *Curr. Opin. Neurobiol.* 20, 156–165. doi: 10.1016/j.conb.2010.02.015

- Engel, A. K., Gerloff, C., Hlilgetag, C. C., and Nolte, G. (2014). Intrinsic coupling modes: multiscale interactions in ongoing brain activity. *Neuron* 80, 867–886. doi: 10.1016/j.neuron.2013.09.038
- Grossman, E. J., and Ingles, M. (2016). The role of thalamic damage in mild traumatic brain injury. *J. Neurotrauma* 33, 163–167. doi: 10.1089/neu.2015.3965
- Guntekin, B., Emek-Savas, D. D., Kurt, P., Yener, G. G., and Basar, E. (2013). Beta oscillatory responses in healthy subjects and subjects with mild cognitive impairment. *Neuroimage Clin.* 3, 39–46. doi: 10.1016/j.nicl.2013.07.003
- Hall, E. L., Woolrich, M. W., Thomaz, C. E., Morris, P. G., and Brookes, M. J. (2013). Using variance information in magnetoencephalography measures of functional connectivity. *Neuroimage* 67, 203–212. doi: 10.1016/j.neuroimage.2012.11.011
- Hillebrand, A., and Barnes, G. R. (2002). A quantitative assessment of the sensitivity of whole-head MEG to activity in the adult human cortex. *Neuroimage* 16, 638–650. doi: 10.1006/nimg.2002.1102
- Hillebrand, A., Prejaas, T., van Dellen, E., Yu, M., Carbo, E. W. S., Douw, L., et al. (2016). Direction of information flow in large-scale resting-state networks is frequency-dependent. *Proc. Natl. Acad. Sci. U.S.A.* 113, 3867–3872. doi: 10.1073/pnas.1515657113
- Hipp, J. F., Hawellek, D. J., Corbetta, M., Siegel, M., and Engel, A. K. (2012). Large-scale cortical correlation structure of spontaneous oscillatory activity. *Nat. Neurosci.* 15, 884–890. doi: 10.1038/nn.3101
- Horn, R. A., and Mathias, R. (1990). An analog of the Cauchy–Schwarz inequality for Hadamard products and unitarily invariant norms. *SIAM J. Matrix Anal. Appl.* 11, 481–498. doi: 10.1137/0611034
- Huang, M. X., Nichols, S., Baker, D. G., Robb, A., Angeles, A., Yurgil, K. A., et al. (2014). Single-subject-based whole-brain MEG slow-wave imaging approach for detecting abnormality in patients with mild traumatic brain injury. *Neuroimage Clin.* 5, 109–119. doi: 10.1016/j.nicl.2014.06.004
- Huang, M. X., Nichols, S., Robb, A., Angeles, A., Drake, A., Holland, M., et al. (2012). An automatic MEG low-frequency source imaging approach for detecting injuries in mild and moderate TBI patients with blast and non-blast causes. *Neuroimage* 61, 1067–1082. doi: 10.1016/j.neuroimage.2012.04.029
- Huang, M. X., Theilmann, R. J., Robb, A., Angeles, A., Nichols, S., Drake, A., et al. (2009). Integrated imaging approach with MEG and DTI to detect mild traumatic brain injury in military and civilian patients. *J. Neurotrauma* 26, 1213–1226. doi: 10.1089/neu.2008.0672
- Hunt, B. A., Tewarie, P. K., Mougou, O. E., Geades, N., Jones, D. K., Singh, K. D., et al. (2016). Relationships between cortical myeloarchitecture and electrophysiological networks. *Proc. Natl. Acad. Sci. U.S.A.* 113, 13510–13515. doi: 10.1073/pnas.1608587113
- Jeter, C. B., Hergenroeder, G. W., Hylin, M. J., Redell, J. B., Moore, A. N., and Dash, P. K. (2013). Biomarkers for the diagnosis and prognosis of mild traumatic brain injury/concussion. *J. Neurotrauma* 30, 657–670. doi: 10.1089/neu.2012.2439
- Kaltainen, H., Helle, L., Liljeström, M., Renvall, H., and Forss, N. (2018). Theta-band oscillations as an indicator of mild traumatic brain injury. *Brain Topogr.* 31, 1037–1046. doi: 10.1007/s10548-018-0667-2
- Kay, T., Harrington, D. E., Adams, R., Anderson, T., Berrol, S., Cicerone, K., et al. (1993). Definition of mild traumatic brain injury. *J. Head Trauma Rehabil.* 8, 86–87.
- Kirkwood, M. W., Yeates, K. O., and Wilson, P. E. (2006). Pediatric sport-related concussion: a review of the clinical management of an oft-neglected population. *Pediatrics* 117, 1359–1371. doi: 10.1542/peds.2005-0994
- Klimesch, W. (2012). α -band oscillations, attention, and controlled access to stored information. *Trends Cogn. Sci.* 16, 606–617. doi: 10.1016/j.tics.2012.10.007
- Leahy, R. M., Mosher, J. C., Spencer, M. E., Huang, M. X., and Lewine, J. D. (1998). A study of dipole localization accuracy for MEG and EEG using a human skull phantom. *Electroencephalogr. Clin. Neurophysiol.* 107, 159–173. doi: 10.1016/S0013-4694(98)00057-1
- Len, T. K., and Neary, J. P. (2011). Cerebrovascular pathophysiology following mild traumatic brain injury. *Clin. Physiol. Funct. Imaging* 31, 85–93. doi: 10.1111/j.1475-097X.2010.00990.x
- Li, L., Arakaki, X., Harrington, M., and Zouridakis, G. (2018). Source connectivity analysis can assess recovery of acute mild traumatic brain injury patients. *Conf. Proc. IEEE Eng. Med. Biol. Soc.* 2018, 3165–3168. doi: 10.1109/EMBC.2018.8513045
- Linás, R. R., Ribary, U., Jeanmonod, D., Kronberg, E., and Mitra, P. P. (1999). Thalamic dysrhythmia: a neurological and neuropsychiatric syndrome characterized by magnetoencephalography. *Proc. Natl. Acad. Sci. U.S.A.* 96, 15222–15227. doi: 10.1073/pnas.96.26.15222
- Luckhoo, H., Hale, J. R., Stokes, M. G., Nobre, C., Morris, P. G., Brookes, M. J., et al. (2012). Inferring task-related networks using independent component analysis in magnetoencephalography. *Neuroimage* 62, 530–541. doi: 10.1016/j.neuroimage.2012.04.046
- Maestú, F., Peña, J. M., Garcés, P., González, S., Bajo, R., Bagic, A., et al., Magnetoencephalography International Consortium of Alzheimer’s Disease (2015). A multicenter study of the early detection of synaptic dysfunction in mild cognitive impairment using magnetoencephalography-derived functional connectivity. *Neuroimage Clin.* 9, 103–109. doi: 10.1016/j.nicl.2015.07.011
- Martinetz, T. M., Berkovich, S. G., and Schulten, K. J. (1993). “Neural-gas” network for vector quantization and its application to time-series prediction. *IEEE Trans. Neural Netw.* 4, 558–569. doi: 10.1109/72.238311
- Nolte, G., Bai, O., Wheaton, L., Mari, Z., Vorbach, S., and Hallett, M. (2004). Identifying true brain interaction from EEG data using the imaginary part of coherency. *Clin. Neurophysiol.* 115, 2292–2307. doi: 10.1016/j.clinph.2004.04.029
- O’Neill, G. C., Bauer, M., Woolrich, M. W., Morris, P. G., Barnes, G. R., and Brookes, M. J. (2015). Dynamic recruitment of resting state sub-networks. *Neuroimage* 115, 85–95. doi: 10.1016/j.neuroimage.2015.04.030
- Oostenveld, R., Fries, P., Maris, E., and Schoffelen, J.-M. (2011). FieldTrip: open source software for advanced analysis of MEG, EEG, and invasive electrophysiological data. *Comput. Intell. Neurosci.* 2011:156869. doi: 10.1155/2011/156869
- Palva, J. M., Wang, S. H., Palva, S., Zhigalov, A., Monto, S., Brookes, M. J., et al. (2018). Ghost interactions in MEG/EEG source space: a note of caution on inter-areal coupling measures. *Neuroimage* 173, 632–643. doi: 10.1016/j.neuroimage.2018.02.032
- Pang, E. W., Dunkley, B. T., Doesburg, S. M., da Costa, L., and Taylor, M. J. (2016). Reduced brain connectivity and mental flexibility in mild traumatic brain injury. *Ann. Clin. Transl. Neurol.* 3, 124–131. doi: 10.1002/acn3.280
- Power, J. D., Cohen, A. L., Nelson, S. M., Wig, G. S., Barnes, K. A., Church, J. A., et al. (2011). Functional network organization of the human brain. *Neuron* 72, 665–678. doi: 10.1016/j.neuron.2011.09.006
- Raichle, M. E., and Mintun, M. A. (2006). Brain work and brain imaging. *Annu. Rev. Neurosci.* 29, 449–476. doi: 10.1146/annurev.neuro.29.051605.112819
- Rapp, P. E., Keyser, D. O., Albano, A., Hernandez, R., Gibson, D. B., Zambon, R. A., et al. (2015). Traumatic brain injury detection using electrophysiological methods. *Front. Hum. Neurosci.* 9:11. doi: 10.3389/fnhum.2015.00011
- Rockland, K. S., and Pandya, D. N. (1979). Laminar origins and terminations of cortical connections of the occipital lobe in the rhesus monkey. *Brain Res.* 179, 3–20. doi: 10.1016/0006-8993(79)90485-2
- Rubinov, M., and Sporns, O. (2010). Complex network measures of brain connectivity: uses and interpretations. *Neuroimage* 52, 1059–1069. doi: 10.1016/j.neuroimage.2009.10.003
- Seeley, W. W., Menon, V., Schatzberg, A. F., Keller, J., Glover, G. H., Kenna, H., et al. (2007). Dissociable intrinsic connectivity networks for salience processing and executive control. *J. Neurosci.* 27, 2349–2356. doi: 10.1523/JNEUROSCI.5587-06.2007
- Sherman, M. A., Lee, S., Law, R., Haegens, S., Thorn, C. A., Hamalainen, M. A., et al. (2016). Neural mechanisms of transient neocortical beta rhythms: converging evidence from humans, computational modeling, monkeys, and mice. *Proc. Natl. Acad. Sci. U.S.A.* 113, E4885–E4894. doi: 10.1073/pnas.1604135113
- Shine, J. M., Bissett, P. G., Bell, P. T., Koyejo, O., Balsters, J. H., Gorgolewski, K. J., et al. (2016). The dynamics of functional brain networks: integrated network states during cognitive task performance. *Neuron* 92, 544–554. doi: 10.1016/j.neuron.2016.09.018
- Sponheim, S. R., McGuire, K. A., Kang, S. S., Davenport, N. D., Aviyente, S., Bernat, E. M., et al. (2011). Evidence of disrupted functional connectivity in the brain after combat-related blast injury. *Neuroimage* 54, S21–S29. doi: 10.1016/j.neuroimage.2010.09.007
- Symons, A. E., El-Dereby, W., Schwartz, M., and Kotz, S. A. (2016). The functional role of neural oscillations in non-verbal emotional communication. *Front. Hum. Neurosci.* 10:239. doi: 10.3389/fnhum.2016.00239

- Tewarie, P., Schoonheim, M. M., Schouten, D. I., Polman, C. H., Balk, L. J., Uitdehaag, B. M. J., et al. (2015). Functional brain networks: linking thalamic atrophy to clinical disability in multiple sclerosis, a multimodal fMRI and MEG Study. *Hum. Brain Mapp.* 36, 603–618. doi: 10.1002/hbm.22650
- Thatcher, R. W., North, D. M., and Biver, C. J. (2008). Development of cortical connections as measured by EEG coherence and phase delays. *Hum. Brain Mapp.* 29, 1400–1415. doi: 10.1002/hbm.20474
- Thornton, K. (2003). The electrophysiological effects of a brain injury on auditory memory functioning: qEEG correlates of impaired memory. *Arch. Clin. Neuropsychol.* 18, 363–378. doi: 10.1093/arclin/18.4.363
- Tzourio-Mazoyer, N., Landeau, B., Papathanassiou, D., Crivello, F., Etard, O., Delcroix, N., et al. (2002). Automated anatomical labeling of activations in SPM using a macroscopic anatomical parcellation of the MNI MRI single-subject brain. *Neuroimage* 15, 273–289. doi: 10.1006/nimg.2001.0978
- Uhlhaas, P. J., Pipa, G., Lima, B., Melloni, L., Neuenschwander, S., Nikolic, D., et al. (2009). Neural synchrony in cortical networks: history, concept and current status. *Front. Integr. Neurosci.* 3:17. doi: 10.3389/neuro.07.017.2009
- Vakorin, V. A., Doesburg, S. M., da Costa, L., Jetly, R., Pang, E. W., and Taylor, M. J. (2016). Detecting mild traumatic brain injury using resting state magnetoencephalographic connectivity. *PLoS Comput. Biol.* 12:e1004914. doi: 10.1371/journal.pcbi.1004914
- van der Naalt, J., van Zomeren, A. H., Sluiter, W. J., and Minderhoud, J. M. (1999). One year outcome in mild to moderate head injury: the predictive value of acute injury characteristics related to complaints and return to work. *J. Neurol. Neurosurg. Psychiatry* 66, 207–213. doi: 10.1136/jnnp.66.2.207
- van Dijk, K. R., Hedden, T., Venkataraman, A., Evans, K. C., Lazar, S. W., and Buckner, R. L. (2010). Intrinsic functional connectivity as a tool for human connectomics: theory, properties, and optimization. *J. Neurophysiol.* 103, 297–321. doi: 10.1152/jn.00783.2009
- Vanderploeg, R. D., Curtiss, G., and Belanger, H. G. (2005). Long-term neuropsychological outcomes following mild traumatic brain injury. *J. Int. Neuropsychol. Soc.* 11, 228–236. doi: 10.1017/S1355617705050289
- Vergara, V. M., Mayer, A. R., Kiehl, K. A., and Calhoun, V. D. (2018). Dynamic functional network connectivity discriminates mild traumatic brain injury through machine learning. *Neuroimage Clin.* 19, 30–37. doi: 10.1016/j.nicl.2018.03.017
- Vidaurre, D., Quinn, A. J., Baker, A. P., Dupret, D., Tejero-Cantero, A., and Woolrich, M. W. (2016). Spectrally resolved fast transient brain states in electrophysiological data. *Neuroimage* 126, 81–95. doi: 10.1016/j.neuroimage.2015.11.047
- von Stein, A., Rappelsberger, P., Sarnthein, J., and Petsche, H. (1999). Synchronization between temporal and parietal cortex during multimodal object processing in man. *Cereb. Cortex* 9, 137–150. doi: 10.1093/cercor/9.2.137
- Ward, L. M. (2003). Synchronous neural oscillations and cognitive processes. *Trends Cogn. Sci.* 7, 553–559. doi: 10.1016/j.tics.2003.10.012
- Weiskopf, N., Lutti, A., Helms, G., Novak, M., Ashburner, J., and Hutton, R. C. (2011). Unified segmentation based correction of R1 brain maps for RF transmit field inhomogeneities (UNICORT). *Neuroimage* 54, 2116–2124. doi: 10.1016/j.neuroimage.2010.10.023
- Wens, V., Marty, B., Mary, A., Op de Beeck, M., Goldman, S., Van Bogaert, P., et al. (2015). A geometric correction scheme for spatial leakage effects in MEG/EEG seed-based functional connectivity mapping. *Hum. Brain Mapp.* 36, 4604–4621. doi: 10.1002/hbm.22943
- Zouridakis, G., Paditar, U., Situ, N., Rezaie, R., Castillo, E., Levin, H., et al. (2012). Functional connectivity changes in mild traumatic brain injury assessed using magnetoencephalography. *J. Mech. Med. Biol.* 12:1240006. doi: 10.1142/S0219519412400064

Conflict of Interest: The authors declare that the research was conducted in the absence of any commercial or financial relationships that could be construed as a potential conflict of interest.

Copyright © 2020 Antonakakis, Dimitriadis, Zervakis, Papanicolaou and Zouridakis. This is an open-access article distributed under the terms of the Creative Commons Attribution License (CC BY). The use, distribution or reproduction in other forums is permitted, provided the original author(s) and the copyright owner(s) are credited and that the original publication in this journal is cited, in accordance with accepted academic practice. No use, distribution or reproduction is permitted which does not comply with these terms.